

## Article

# Targeted Deletion of Thymosin Beta 4 in Hepatic Stellate Cells Ameliorates Liver Fibrosis in a Transgenic Mouse Model

Jieun Kim <sup>1,2,†</sup>, Chanbin Lee <sup>1,2,†</sup>, Jinsol Han <sup>2</sup> , Hyeong Jeong <sup>2</sup>, Sihyung Wang <sup>3</sup>, Yung Hyun Choi <sup>4</sup>   
and Youngmi Jung <sup>2,5,\*</sup> 

- <sup>1</sup> Institute of System Biology, Pusan National University, Pusan 46241, Republic of Korea; jieun@pusan.ac.kr (J.K.); chanbin@pusan.ac.kr (C.L.)  
<sup>2</sup> Department of Integrated Biological Science, College of Natural Sciences, Pusan National University, Pusan 46241, Republic of Korea; wlsthf1408@pusan.ac.kr (J.H.); jeong17@pusan.ac.kr (H.J.)  
<sup>3</sup> New Drug Development Center, Daegu Gyeongbuk Medical Innovation Foundation, Daegu 41061, Republic of Korea; shwang@kmedihub.re.kr  
<sup>4</sup> Department of Biochemistry, Dong-Eui University College of Korean Medicine, Pusan 47227, Republic of Korea; choiyh@deu.ac.kr  
<sup>5</sup> Department of Biological Sciences, College of Natural Sciences, Pusan National University, Pusan 46241, Republic of Korea  
\* Correspondence: yjung@pusan.ac.kr; Tel.: +82-51-510-2262  
† These authors contributed equally to this work.

**Abstract:** Liver fibrosis is the most common feature of liver disease, and activated hepatic stellate cells (HSCs) are the main contributors to liver fibrosis. Thus, finding key targets that modulate HSC activation is important to prevent liver fibrosis. Previously, we showed that thymosin  $\beta 4$  (T $\beta 4$ ) influenced HSC activation by interacting with the Hedgehog pathway in vitro. Herein, we generated T $\beta 4$  conditional knockout (T $\beta 4$ -flox) mice to investigate in vivo functions of T $\beta 4$  in liver fibrosis. To selectively delete T $\beta 4$  in activated HSCs, double-transgenic (DTG) mice were generated by mating T $\beta 4$ -flox mice with  $\alpha$ -smooth muscle actin ( $\alpha$ -Sma)-Cre-ER<sup>T2</sup> mice, and these mice were administered carbon tetrachloride (CCl<sub>4</sub>) or underwent bile duct ligation to induce liver fibrosis. T $\beta 4$  was selectively suppressed in the activated HSCs of DTG mouse liver, and this reduction attenuated liver injury, including fibrosis, in both fibrotic models by repressing Hedgehog (Hh) signaling. In addition, the re-expression of T $\beta 4$  by an adeno-associated virus reversed the effect of HSC-specific T $\beta 4$  deletion and led to liver fibrosis with Hh activation in CCl<sub>4</sub>-exposed mice treated with tamoxifen. In conclusion, our results demonstrate that T $\beta 4$  is a crucial regulator of HSC activation, suggesting it as a novel therapeutic target for curing liver fibrosis.

**Keywords:** T $\beta 4$ ; T $\beta 4$ -flox transgenic mice; hepatic stellate cells; liver fibrosis



**Citation:** Kim, J.; Lee, C.; Han, J.; Jeong, H.; Wang, S.; Choi, Y.H.; Jung, Y. Targeted Deletion of Thymosin Beta 4 in Hepatic Stellate Cells Ameliorates Liver Fibrosis in a Transgenic Mouse Model. *Cells* **2023**, *12*, 1658. <https://doi.org/10.3390/cells12121658>

Academic Editor: Kuo Du

Received: 28 April 2023

Revised: 6 June 2023

Accepted: 16 June 2023

Published: 18 June 2023



**Copyright:** © 2023 by the authors. Licensee MDPI, Basel, Switzerland. This article is an open access article distributed under the terms and conditions of the Creative Commons Attribution (CC BY) license (<https://creativecommons.org/licenses/by/4.0/>).

## 1. Introduction

Liver fibrosis, which is scarring of the liver, is the most common consequence of liver injuries, including excessive fat accumulation, viral infection, alcohol consumption, and cholestasis [1]. The activation of hepatic stellate cells (HSCs) is the substantial event in the development and progression of liver fibrosis, and activated/myofibroblastic HSCs are mainly responsible for the synthesis and infiltration of the extracellular matrix (ECM), such as collagens [1–3]. Thus, controlling HSC activation is considered an important strategy to alleviate chronic liver disease, including liver fibrosis; however, the key factors that target and control HSC activation remain to be fully elucidated.

Thymosin beta 4 (T $\beta 4$ ), a naturally occurring peptide containing 43 amino acids, is a member of the highly conserved thymosin beta family [4,5]. This endogenous peptide is produced in higher concentrations where tissues are damaged and modulates multiple cellular activities, including cell motility, survival, wound healing, and inflammation [4,6–8].

Tβ4 is regarded as a multifunctional regenerative peptide, and many researchers and companies have attempted to develop a synthetic copy of Tβ4 as a novel regenerative medicine to treat various diseases, such as dermal wounds, corneal injuries, cardiovascular disease, and neurological disorders [4,9]. In experimental animal studies, exogenous Tβ4 administration has been shown to have beneficial effects on myocardial infarction, stroke, hair loss, and dry eye [4,9–12]. There have also been several clinical trials assessing synthetic Tβ4 treatment in dry eye syndrome and neurotrophic keratitis [13–15]. However, there is still a huge limitation in the application of Tβ4 as a treatment because many studies have only focused on the visible effects of exogenous or synthetic Tβ4, but not endogenous Tβ4, and have overlooked the underlying importance of endogenous Tβ4 under physiological and pathophysiological conditions [5]. Therefore, the functions of Tβ4 produced but not supplemented in the body remain unknown.

Accumulating evidence suggests that Tβ4 is involved in the development of hepatic fibrosis and is specifically associated with HSC activation [5,16,17]. As with Tβ4 studies in other organs, most experimental studies have focused on the actions of exogenous Tβ4 on liver fibrosis and reported that exogenous Tβ4 could attenuate liver fibrosis by modulating HSC activation [5,18–20]. However, until recently, researchers have been interested in the roles of endogenous Tβ4 in the liver. Our previous studies revealed that Tβ4 is expressed by activated HSCs in the chronically injured liver and impacts HSC activation and liver fibrosis by directly interacting with Hedgehog (Hh) signaling, which is a main controller of HSC activation and fibrosis [16,17]. In vitro suppression of Tβ4 decreased the expression of smoothed (Smo), an effector of the Hh pathway, and GLI family zinc finger 2 (Gli2), a transcription factor in the Hh pathway, and it inactivated HSCs, suggesting that Tβ4 was a potential regulator of HSC activation [16]. However, these findings were obtained from in vitro experiments, and it remains a significant challenge to investigate the in vivo effect of Tβ4 on liver fibrosis in the context of Tβ4 suppression because of the absence of available Tβ4-knockout mice.

In the current study, we created Tβ4 conditional knockout (Tβ4-flox) mice harboring floxed Tβ4 alleles by using the Cre-LoxP system. To induce activated HSC-targeted Tβ4 knockout, double-transgenic (DTG) mice were obtained by mating Tβ4-flox mice with α-smooth muscle actin (α-Sma)-Cre-ER<sup>T2</sup> mice with tamoxifen-inducible Cre activity under the control of the α-Sma promoter [21,22]. α-Sma is a marker of activated HSCs [3,22]. Based on our previous findings showing that Tβ4 was primarily expressed by activated HSCs and that Tβ4 suppression in HSCs inhibited HSC activation [16,17], we investigated the physiological function of activated HSC-specific deletion of Tβ4 in the experimental liver fibrosis models. Herein, we demonstrate that HSC-targeted Tβ4 depletion attenuates the activation of HSCs and hepatic fibrosis, suggesting Tβ4 as an attractive target to develop therapeutic agents for liver fibrosis and that Tβ4-flox mice are a useful experimental model for use in future studies to further understand the functions of endogenous Tβ4 in other diseases and organs.

## 2. Materials and Methods

### 2.1. Generation of Tβ4-Floxed Mice

The conditional knock-out Tβ4 mice were generated by MacroGen, Inc. using CRISPR/Cas9 system and were maintained in pathogen-free condition at MacroGen (Seoul, Republic of Korea). Cas9 nuclease (M0386; New England Biolabs Inc., Ipswich, MA, USA) and guide RNAs (gRNAs) to target intron 1–2 and intron 2–3 of Tβ4 gene were prepared by MacroGen using GeneArt<sup>TM</sup> Precision gRNA Synthesis Kit (A29377, Thermo Fisher Scientific, Waltham, MA, USA). Double-stranded donor DNA (dsDonor) was synthesized from Invitrogen. Two sets of gRNAs (gRNA#1: ACG AAG GTG GAA ATA GTC AAA GG, gRNA#2: TTA GCA TGT CTT GCT TAG CGA GG) were synthesized and validated activity using in vitro cleavage reactions. Briefly, amplified Tβ4 gene as template was incubated for 90 min at 37 °C with Cas9 nuclease (20 nm) and gRNA (40 nm) in 1 × NEB 3 buffer. Reactions were terminated with 6 × stop solution containing 30% glycerol, 1.2% SDS,

and 100 mM EDTA. Mixtures were performed electrophoresis and confirmed cleavage activity. After confirming in vitro cleavage reactions, microinjection of CRISPR/Cas9 was performed. Briefly, pregnant mare serum gonadotropin (PMSG) and human chorionic gonadotropin (hCG) were treated into C57BL/6N female mice. After 48 h, these female mice were mated with C57BL/6N stud male mice. Next day, female mice showing vaginal plug were sacrificed, and fertilized embryos are harvested. The mixture of Cas9 nuclease, two sets of sgRNAs, and dsDonor were microinjected into one cell embryo. Microinjected embryos were incubated at 37 °C for 2 h and then microinjected embryos at the 14-to-16-cell stage were transplanted into oviducts of pseudo-pregnant recipient mice. After F0 founders were born, genotyping for loxP insertion was performed with a set of 2 primers (Forward primer: GGG GGA TGC TAA ACT CTT CC; Reverse primer: ACC CAG CTT TTT CCT TCA CC) and the expected PCR fragment size is 1802-bp. Then, the fragment was digested with AflIII restriction enzyme to confirm the positive sample. Enzyme-digested positive samples were performed via TA cloning and analyzed by Sequencing. After breeding of F0 founders by MacroGen, we obtained the T $\beta$ 4<sup>flox/+</sup> offspring from MacroGen (Seoul, Republic of Korea) and maintained these mice over generations.

## 2.2. Animal Experiments

Male C57BL/6 mice (6-week-old mice) were purchased from Hyochang (Daegu, Republic of Korea) and used for wild-type (WT) controls. All mice were provided an adequate acclimation period to allow them to stabilize to their new environment. The  $\alpha$ -Sma-Cre-ER<sup>T2</sup> transgenic mice, which are originally made by Dr. Pierre Chambon (IGBMC), were kindly provided by Dr. Anna Mae Diehl (Duke University Medical Center) [21,22]. Cre-positive and homozygous T $\beta$ 4<sup>flox/flox</sup> DTG mice were bred by crossing  $\alpha$ -Sma-Cre-ER<sup>T2</sup> hemizygous, T $\beta$ 4<sup>flox/flox</sup> homozygous mice with T $\beta$ 4<sup>flox/flox</sup> homozygous mice (T $\beta$ 4-flox mice). Genotyping for  $\alpha$ -Sma-Cre-ER<sup>T2</sup> was performed using a set of 4 primers (PB003: TGC AAC GAG TGA GGT TCG C; PB004: GAT CCT GGC AAT TTC GGC TAT ACG; 1136: GGT TTC TAT TGC TAC CAA GAG ACA T; 1044: TGC ACC AAA CCC TGG ACT AAG CAT). Genotyping for the floxed T $\beta$ 4 allele was performed using a set of 2 primers (Forward primer: GGA AAT GGC TTC GAT CTA TCC; Reverse primer: CGA GTC CTC TCT AAA GAT CTT CC). After genotyping, each newly weaned DTG mice were randomly introduced in a clean cage. All mice were housed in groups (maximum of 5 mice per cage) in ventilated, temperature- and humidity-controlled cages with an absorbent bedding material under a 12 h light/12 h dark cycle with free access to standard food and water. All animals were treated the same way, and the time of treatment was always the same.

For the induction of toxic liver fibrosis, 7-week-old C57BL/6 WT or DTG male mice were treated with four intraperitoneal injections of 100  $\mu$ L of CCl<sub>4</sub> (0.5  $\mu$ L per g body weight, dissolved in corn oil) or corn oil (CON) ( $n = 4$ –5 mice per group), as described previously [23]. Animals were sacrificed at 2 days after the last CCl<sub>4</sub> injection. For the induction of cholestatic liver fibrosis, 8-week-old DTG male mice were subjected to either BDL or sham surgery under isoflurane anesthesia ( $n = 4$ –5 mice per group), as described previously [22]. Animals were sacrificed at 3 weeks after surgery. To initiate Cre-mediate gene rearrangement of floxed allele in CCl<sub>4</sub> model, mice were injected intraperitoneally with tamoxifen (TMX, Sigma-Aldrich, St. Louis, MO, USA) dissolved in corn oil. In CCl<sub>4</sub> model,  $\alpha$ -Sma-Cre-ER<sup>T2</sup> activity was induced by 6 intraperitoneal injections of TMX (2 mg per mice) starting 3 days after the first CCl<sub>4</sub> injection and ending one day before the last CCl<sub>4</sub> injection as previously described [23]: CON + VEH ( $n = 4$ ), CON + TMX ( $n = 4$ ), CCl<sub>4</sub> + VEH ( $n = 5$ ), and CCl<sub>4</sub> + TMX ( $n = 5$ ). In BDL model, TMX (10 mg per kg body weight) was delivered every other day (total of 9 intraperitoneal injections) starting at 4 days after the BDL surgery until 3 weeks after surgery as previously described [22]: Sham + VEH ( $n = 4$ ), Sham + TMX ( $n = 4$ ), BDL + VEH ( $n = 5$ ), and BDL + TMX ( $n = 5$ ). To assess the effect of T $\beta$ 4 re-expression in the livers of TMX-treated DTG mice, AAV6 vectors containing a T $\beta$ 4 gene were used to conditionally enhance the T $\beta$ 4 expression in the liver, mainly HSCs [24]. Under the identical CCl<sub>4</sub> and TMX regimen, DTG mice were

intravenously injected via tail vein with  $5 \times 10^{10}$  viral genome copies of AAV6-CMV-Con or AAV6-CMV-T $\beta$ 4 (Vector Biolabs) after 3rd injection of CCl<sub>4</sub>, and then they received residual TMX and T $\beta$ 4 injections: CON + VEH + AAV6-Con, CCl<sub>4</sub> + VEH + AAV6-Con, CCl<sub>4</sub> + TMX + AAV6-Con, and CCl<sub>4</sub> + TMX + AAV6-T $\beta$ 4 ( $n = 4$  per group). Vector injections were performed slowly, and the volume was limited to 100 $\mu$ L for tail vein injection. At the end of each time point, mice were sacrificed to collect blood and liver samples. Animal care and surgical procedures were approved by the Pusan National University–Institutional Animal Care and Use Committee and carried out in accordance with the provisions of the National Institutes of the National Institutes of Health Guide for the Care and Use of Laboratory Animals (Approval Number PNU-2016-1286 and PNU-2020-2652).

### 2.3. RNA Analysis

Total RNA was extracted from pHSCs or liver tissues using Trizol reagent (Invitrogen, Carlsbad, CA, USA). The concentration and purity of RNA were determined using nanodrop. Template complementary DNA was synthesized from total RNA using the SuperScript II First-strand synthesis system (Invitrogen, Carlsbad, CA, USA) according to the manufacturer's protocols. Real-time qRT-PCR analysis was performed on QuantStudio 1 (Thermo Scientific, Pleasanton, CA, USA) using POWER SYBR Green Master Mix (Applied Biosystems, Foster City, CA, USA) on the manufacturer's instructions. All reactions were duplicated, and data were analyzed according to the  $\Delta\Delta$ Ct method. The expression values were normalized to the levels of mouse 40S ribosomal protein S9 mRNA. The sequences of all primers used in this study are summarized in Table S1. All PCR products were directly sequenced for genetic confirmation (Macrogen, Inc., Seoul, Republic of Korea).

### 2.4. Western Blot Assay

Total protein was extracted from pHSCs or freeze-clamped liver tissues that had been stored at  $-80$  °C. Samples were homogenized in triton lysis buffer supplemented with protease inhibitors (Complete mini; Roche, Indianapolis, IN, USA) and centrifuged at 13,000 r.c.f. for 15 min. The supernatants containing protein extracts were used in subsequent biochemical analysis. Protein concentration was measured by Pierce BCA Protein Assay Kit (Thermo Fisher Scientific, Waltham, MA, USA). Equal amount of total protein lysates was separated by SDS–polyacrylamide gel electrophoresis (PAGE) and then transferred onto a polyvinylidene difluoride (PVDF) membrane (Millipore, Darmstadt, Germany). Primary antibodies used in this study were as follows: rabbit anti-T $\beta$ 4 antibody (A9520; diluted 1:5000; Immundiagnostik AG, Bensheim, Germany), rabbit anti-Smo antibody (ab72130; diluted 1:1000; Abcam, Cambridge, MA, USA), rabbit anti-Gli2 antibody (GWB-CE7858; diluted 1:1000; GenWay Biotech, Inc., San Diego, CA, USA), rabbit anti-pGSK-3 $\alpha$ / $\beta$  antibody (9331; diluted 1:1000; Cell Signaling Technology, Inc., Danvers, MA, USA), rabbit anti-GSK-3 $\beta$  antibody (9315; diluted 1:1000; Cell Signaling Technology, Inc., Danvers, MA, USA), rabbit anti-TGF- $\beta$  antibody (3711S; diluted 1:1000; Cell Signaling Technology, Inc., Danvers, MA, USA), mouse anti-Cre Recombinase antibody (MAB3120; diluted 1:500; Sigma-Aldrich, St. Louis, MO, USA), mouse anti-ILK antibody (611802; diluted 1:1000; BD Biosciences, San Diego, CA, USA), mouse anti- $\alpha$ -Sma antibody (A5228; diluted 1:1000; Sigma-Aldrich, St. Louis, MO, USA), and mouse anti-GAPDH antibody (MCA4739; diluted 1:1000; AbD Serotec, Oxford, UK). Horseradish peroxidase-conjugated anti-rabbit or anti-mouse IgG (Enzo Life Sciences, Inc., Farmingdale, NY, USA) was used as secondary antibody. Protein bands were detected using an EzWestLumi ECL solution (ATTO Corporation, Tokyo, Japan) as per the manufacturer's specifications (ATTO Corporation, Ez-Capture II, Tokyo, Japan). Densities of protein bands were measured using CS Analyzer software (Version 3.00.1011, ATTO & Rise Corporation, Tokyo, Japan).

### 2.5. Liver Histology and Immunohistochemistry

Liver specimens were fixed in 10% neutral buffered formalin, embedded in paraffin, and cut into 4  $\mu$ m sections and placed on glass slides. To examine hepatic morphology

and assess liver fibrosis, liver sections were deparaffinized, rehydrated, and stained via the usual method with standard hematoxylin and eosin staining (H&E) and Sirius red staining as previously described [16,25]. For immunohistochemical staining, liver sections were deparaffinized, rehydrated, and then incubated for 10 min in 3% hydrogen peroxide to block endogenous peroxidase. Antigen retrieval was performed by heating in 10 mM sodium citrate buffer (pH 6.0). Sections were blocked in DAKO protein block (X9090; DAKO, Carpinteria, CA, USA) for 30 min and incubated with primary antibodies at 4 °C overnight. The following primary antibodies were used: T $\beta$ 4 (A9520; diluted 1:8000; Immundiagnostik AG, Bensheim, Germany) and  $\alpha$ -Sma (ab5694; diluted 1:1000; Abcam, Cambridge, MA, USA). Polymer horseradish peroxidase (HRP)-conjugated anti-rabbit secondary antibody (K4003; DAKO, Carpinteria, CA, USA) was used as secondary antibody. 3,3'-Diaminobenzidine (DAB) (K3466; DAKO, Carpinteria, CA, USA) was employed for the detection procedure.

### 2.6. HSC Isolation and Culture

Primary HSCs were isolated as described previously [16,25]. Briefly, mice were anaesthetized with isoflurane to immobilize in the recumbent position on a treatment table, and the inferior vena cava was cannulated under aseptic conditions. Livers were perfused in situ with EGTA and collagenase (Sigma-Aldrich, St. Louis, MO, USA), to disperse the cells. Primary HSCs were separated by differential centrifugation on OptiPrep (Sigma-Aldrich, St. Louis, MO, USA) density gradient and located on the upper layer of 11.5% OptiPrep. The purity of HSCs was >98%, as established by microscopy examination for lipid droplets and vitamin A auto-fluorescence. Isolated HSCs were seeded at a density of  $3 \times 10^2$  cells/mm<sup>2</sup> and cultured in DMEM medium (Gibco, Thermo Fisher Scientific, Waltham, MA, USA) supplemented with 10% FBS and 1% P/S at 37 °C in a humidified atmosphere containing 5% CO<sub>2</sub>.

### 2.7. Adenoviral Transfection in Primary HSCs Isolated from Mice

HSCs isolated from T $\beta$ 4-flox male mice were cultured for 3 days, and then starved in serum-depleted medium for overnight. Adenoviruses harboring either the GFP gene (AdGFP, Vector Biolabs, Malvern, PA, USA) or Cre recombinase gene (AdCre, Vector Biolabs, Malvern, PA, USA) were added to these pHSCs at a multiplicity of infection (MOI) of 80, as described previously [16]. After 24 h, virus-containing medium was aspirated and replaced with fresh medium. Viral efficiency of AdGFP infection was assessed by fluorescent microscope, with >95% of infected cells found to be GFP positive.

### 2.8. Measurement of ALT and AST

Serum aspartate aminotransferase (AST/GOT, glutamate-oxaloacetate transaminase) and alanine aminotransferase (ALT/GPT, glutamate pyruvate transaminase) were measured using GOT reagents (AM103-K; Asan Pharmaceutical, Seoul, Republic of Korea) and GPT reagents (AM102-K; Asan Pharmaceutical, Seoul, Republic of Korea) according to the manufacturer's instructions.

### 2.9. Hydroxyproline Assay

Hydroxyproline content of the livers was calculated by the method previously described [16,25]. Briefly, 50 mg of freeze liver tissue was hydrolyzed in 6N HCl at 110 °C for 16 h. The hydrolysate was evaporated under vacuum and the sediment was re-dissolved in 1 mL distilled water. Sample were filtered using 0.22  $\mu$ m filter centrifuge tube (Corning Incorporated) at 14,000 r.p.m. for 5 min. Then, 0.5 mL of chloramine-T solution, containing 1.41 g of chloramine-T dissolved in 80 mL of acetate-citrate buffer and 20 mL of 50% isopropanol, was added and incubated at room temperature for 20 min. Then, 0.5 mL of Ehrlich's solution, containing 7.5 g of dimethylaminobenzaldehyde dissolved in 13 mL of 60% perchloric acid and 30 mL of isopropanol, was added to the mixture and incubated at 65 °C for 15 min. After cooling at room temperature, the standard and samples were

measured by a spectrophotometer at 561 nm. Amount of hydroxyproline in each sample was determined using regression curve from high purity Trans-4-hydroxy-L-proline (Sigma-Aldrich, St. Louis, MO, USA) as a standard. Total hydroxyproline was calculated based on individual liver weights (mg hydroxyproline/mg liver).

### 2.10. Statistics

Results are expressed as mean  $\pm$  s.e.m. Statistical analysis was analyzed by two-tailed unpaired Student's *t*-test. Differences were considered as statistically significant when *p*-values < 0.05. Statistical analyses were performed using Microsoft Excel and GraphPad Prism 8 (GraphPad Software Inc., Boston, MA, USA).

## 3. Results

### 3.1. Generation of T $\beta$ 4 Conditional Knockout Mice

To elucidate the precise function of T $\beta$ 4 *in vivo*, we generated T $\beta$ 4 conditional knockout mice harboring the floxed T $\beta$ 4 allele by CRISPR/Cas9-mediated gene editing (Figure 1A). To insert flanking loxP sites, exon 2 of T $\beta$ 4 was chosen as the target for conditional deletion because exon 2 encompasses approximately 75% of the coding sequence, includes the start codon, and encodes 33 amino acids of the 43-amino acid T $\beta$ 4 protein. Thus, the removal of exon 2 is highly likely to cause a deletion and frameshift, resulting in a null allele. Two different CRISPR gRNAs (gR#1 and gR#2) were designed to separately target the distinct locations of T $\beta$ 4 introns 1–2 and 2–3, respectively, producing the floxed T $\beta$ 4 allele (Figure S1). To obtain homozygous T $\beta$ 4<sup>flox/flox</sup> mice, hemizygous T $\beta$ 4<sup>flox/+</sup> mice were interbred, and the offspring were genotyped by PCR. The presence of the loxP site was detected in the transgenic mice (Figure 1B). Among these mice, hemizygous T $\beta$ 4<sup>flox/+</sup> mice had wild-type (wt, 195 bp) and mutant (229 bp) forms of the T $\beta$ 4 allele, and homozygous T $\beta$ 4<sup>flox/flox</sup> (T $\beta$ 4-flox) mice contained only the T $\beta$ 4 mutant allele. Homozygous T $\beta$ 4<sup>flox/flox</sup> mice appeared normal, were fertile, and were born at the expected Mendelian ratio.

Because T $\beta$ 4 has been shown to be mainly expressed by activated HSCs [16,17], primary HSCs (pHSCs) were isolated from T $\beta$ 4-flox mice and cultured for 7 days to facilitate spontaneous activation and check whether T $\beta$ 4 could be deleted by the Cre-LoxP system in these cells. On Day 4, pHSCs were treated with adenoviral vectors having Cre recombinase (AdCre) or green fluorescent protein (AdGFP). Compared with freshly isolated pHSCs (Day 0), AdGFP-treated pHSCs had significantly increased levels of T $\beta$ 4 on Day 7, as measured by qRT-PCR (Figure 1C). However, the T $\beta$ 4 RNA level in pHSCs treated with AdCre was remarkably decreased compared with that in AdGFP-exposed pHSCs. These results validate the efficacy of T $\beta$ 4 deletion by using T $\beta$ 4-flox mice and suggest that T $\beta$ 4-flox mice are available tools to conditionally knock out T $\beta$ 4 *in vivo*.

### 3.2. HSC-Targeted Knockout of T $\beta$ 4 Prevents Liver Fibrosis in Mice

After confirming the successful deletion of T $\beta$ 4 by the Cre-LoxP system in pHSCs isolated from T $\beta$ 4-flox mice, we examined the physiological function of T $\beta$ 4 in the liver by generating double-transgenic (DTG) mice in which T $\beta$ 4 could be selectively deleted in activated HSCs *in vivo*. Because  $\alpha$ -Sma is a reliable and widely used marker of activated/myofibroblastic HSCs [3,22],  $\alpha$ -Sma-Cre-ER<sup>T2</sup> mice in which tamoxifen (TMX)-inducible Cre activity is influenced by the  $\alpha$ -Sma promoter were mated with T $\beta$ 4-flox mice, generating DTG mice. The offspring from this mating were genotyped to determine the presence of the Cre transgene and the floxed T $\beta$ 4 allele (data not shown). Thereafter, Cre-positive and homozygous T $\beta$ 4<sup>flox/flox</sup> DTG mice were used for the next experiment.

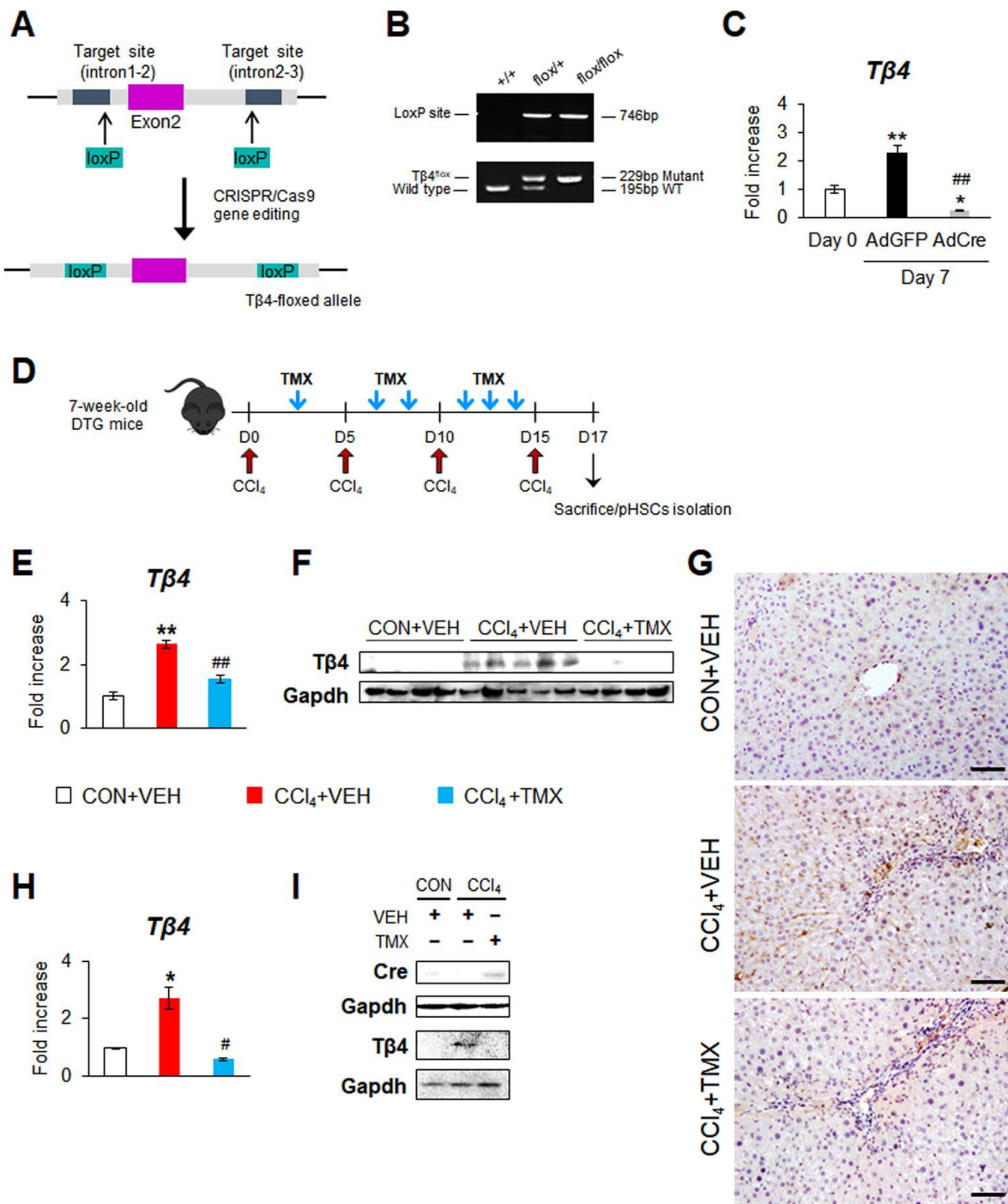


**Figure 1.** Generation of the *Tβ4*-floxed mice and tamoxifen-induced *Tβ4* deletion in CCl<sub>4</sub>-injected DTG mice and primary HSCs isolated from these mice. (A) Schematic illustration to generate a conditional allele at the *Tβ4* locus. Intron 1–2 and Intron 2–3 of *Tβ4* gene was targeted by two guide RNAs that were designed to cut both ends of the exon 2 of *Tβ4*. By CRISPR/Cas9 gene editing tool, two LoxP sequences are inserted at both ends of the exon 2 by single-stranded donor oligonucleotides, generating the *Tβ4*-floxed allele having target exon 2 with flanking loxP sites. (B) PCR-based genotyping for the LoxP site and the floxed *Tβ4* alleles. Genomic DNA extracted from mice were amplified using specific primers. Wild-type *Tβ4*<sup>+/+</sup>, hemizygous *Tβ4*<sup>lox/+</sup>, and homozygous *Tβ4*<sup>lox/lox</sup> (*Tβ4*-floxed) mice were clearly distinguished by detecting the presence of LoxP site (746-bp size in product) and the floxed *Tβ4* allele (WT: 195-bp, mutant: 229-bp size in product). (C) qRT-PCR analysis of *Tβ4* in primary mouse HSCs (pHSCs) at Day 0 and AdGFP or AdCre-transfected pHSCs at Day 7. These cells were isolated from livers of *Tβ4*-floxed mice. Results are

normalized to pHSCs at Day 0. Results of relative expression values are graphed as mean  $\pm$  s.e.m. of triplicate experiments (Student's *t*-test; \*  $p < 0.05$ , \*\*  $p < 0.005$  vs. Day0, <sup>##</sup>  $p < 0.005$  vs. AdGFP) (D) Schematic diagram showing the timing of carbon tetrachloride (CCl<sub>4</sub>) and tamoxifen (TMX) injection into double-transgenic (DTG) mice. At 2 days after the last injection of CCl<sub>4</sub>, mice were sacrificed to harvest tissue samples or isolate primary HSC (pHSC). (E) qRT-PCR analysis of hepatic Tβ4 in representative DTG mice receiving corn oil (CON) + vehicle (VEH) ( $n = 4$ ), CCl<sub>4</sub> + VEH ( $n = 5$ ), or CCl<sub>4</sub> + TMX ( $n = 4$ ). (F) Representative immunoblots of hepatic Tβ4 in representative mice from each group, CON + VEH ( $n = 4$ ), CCl<sub>4</sub> + VEH ( $n = 5$ ), and CCl<sub>4</sub> + TMX ( $n = 4$ ). Gapdh was used as an internal control. (G) Representative images of immunostaining for Tβ4 in liver sections from each group (scale bar = 50 μm). (H) qRT-PCR analysis of Tβ4 in pHSCs isolated from livers of representative mice from each group ( $n = 3$  per group). Results of relative expression values are graphed as mean  $\pm$  s.e.m. (Student's *t*-test; \*  $p < 0.05$ , \*\*  $p < 0.005$  vs. CON + VEH group, <sup>#</sup>  $p < 0.05$ , <sup>##</sup>  $p < 0.005$  vs. CCl<sub>4</sub> + VEH group). (I) Immunoblots of Cre and Tβ4 in pHSCs isolated from livers of mice from each group. Gapdh was used as an internal control. Immunoblots shown represent one of three experiments with similar results.

To test the effect of Cre-mediated Tβ4 deletion *in vivo* and investigate the function of Tβ4 in HSCs, we first used a carbon tetrachloride (CCl<sub>4</sub>)-induced liver fibrosis model (Figure S2A). In the experimental animal model of liver fibrosis, liver morphology was distorted, and the levels of serum alanine aminotransferase (ALT) and aspartate aminotransferase (AST) were significantly elevated in CCl<sub>4</sub>-exposed mice compared with corn oil-treated mice (Figure S2B,C). Distinct liver fibrosis was confirmed by the accumulation of collagen and higher amounts of hepatic hydroxyproline, which is a biochemical measurement quantifying liver fibrosis, and α-Sma in mice treated with CCl<sub>4</sub> than mice treated with corn oil (Figure S2B–D). Tβ4 was also elevated in the fibrotic group (Figure S2D). After confirming that CCl<sub>4</sub> induced severe hepatic fibrosis in mice, DTG mice receiving CCl<sub>4</sub> or corn oil (CON) were intraperitoneally injected with TMX to knockout Tβ4 (Figure 1D). The same volume of vehicle (VEH) with TMX was given to the CON + VEH and CCl<sub>4</sub> + VEH groups. The hepatic Tβ4 level was significantly elevated in the CCl<sub>4</sub> + VEH group compared with that in the CON + VEH group, but the level of Tβ4 apparently declined in the CCl<sub>4</sub> + TMX group, as examined by qRT-PCR and immunoblotting (Figure 1E,F). Immunohistochemistry staining for Tβ4 presented that the hepatic accumulation of Tβ4-positive cells was markedly reduced in the CCl<sub>4</sub> + TMX group compared with the CCl<sub>4</sub> + VEH group (Figure 1G). Consistent with our previous findings [16,17], the livers in the CON + VEH group hardly expressed Tβ4 (Figure 1E–G). TMX itself did not influence hepatic Tβ4 expression (data not shown). To examine the selective deficiency of Tβ4 in HSCs, Tβ4 expression was measured in the pHSCs isolated from these mice. As expected, qRT-PCR and immunoblot analyses showed that in pHSCs, the Tβ4 level was significantly higher in the CCl<sub>4</sub> + VEH group than the CON + VEH group, whereas this level greatly decreased in the CCl<sub>4</sub> + TMX group, which had enhanced Cre expression compared to the CCl<sub>4</sub> + VEH group (Figure 1H,I). These data suggest that TMX successfully induced Cre expression, which selectively deleted Tβ4 in HSCs *in vivo*.

We investigated whether HSC-targeted Tβ4 deletion influenced the liver response to CCl<sub>4</sub>-induced damage. H&E staining and Sirius red staining revealed that severe hepatic injury and fibrotic nodules were alleviated in the CCl<sub>4</sub> + TMX group compared with the CCl<sub>4</sub> + VEH group (Figure 2A, top and middle panel). The increases in liver weight-to-body weight (LW/BW) ratio, levels of serum ALT/AST, and hydroxyproline contents in the CCl<sub>4</sub> + VEH group were significantly reduced in the CCl<sub>4</sub> + TMX group (Figure 2B–D). Immunohistochemistry staining for α-Sma presented that the apparent accumulation of α-Sma-expressing HSCs in the liver in the CCl<sub>4</sub> + VEH group was markedly mitigated in the CCl<sub>4</sub> + TMX group (Figure 2A, bottom panel). Fibrotic changes in these mice were confirmed by Western blot analysis, which showed that the significant increase in the HSC activation markers α-Sma and Col1α1 in the CCl<sub>4</sub> + VEH group compared with the



CON + VEH group was significant or tended to be alleviated in the livers of the CCl<sub>4</sub> + TMX group (Figure 2E,F). In addition, pHSCs from the CCl<sub>4</sub> + TMX group had significantly lower levels of α-Sma and transforming growth factor beta (Tgf-β) than those in cells from the CCl<sub>4</sub> + VEH group (Figure 2G,H). TMX itself did not influence liver function, histomorphology, or fibrosis (Figure S3).

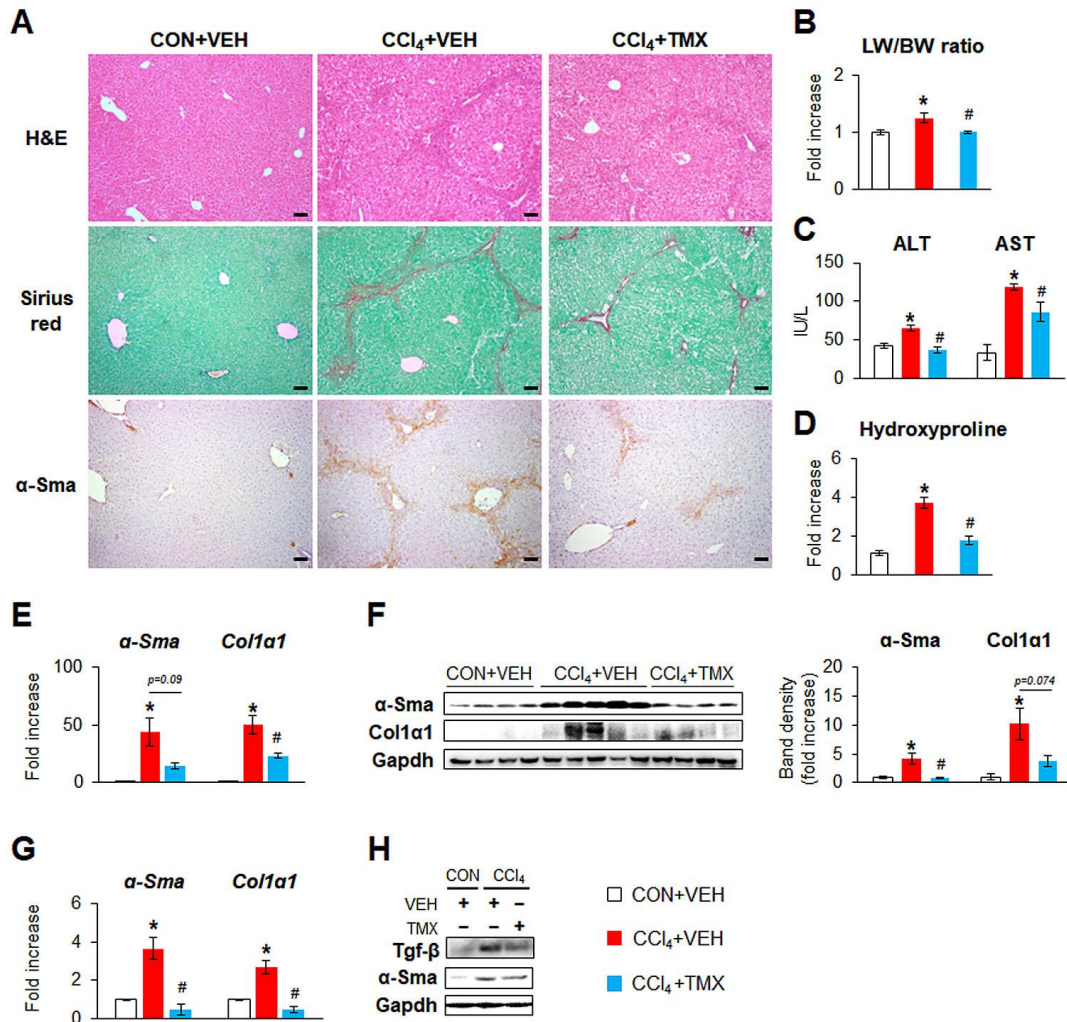


**Figure 2.** HSC-targeted Tβ4 deletion alleviates CCl<sub>4</sub>-induced liver injury and fibrosis. (A) Representative images of hematoxylin and eosin (H&E) staining, Sirius red staining, and immunostaining for α-Sma in liver sections from DTG mice receiving corn oil (CON) + vehicle (VEH), carbon tetrachloride (CCl<sub>4</sub>) + VEH, or CCl<sub>4</sub> + tamoxifen (TMX) (scale bar = 50 μm). (B) Relative ratio of liver weight to body weight (LW/BW), (C) serum levels of ALT and AST, and (D) hepatic hydroxyproline contents in livers of all mice from each group. (E) qRT-PCR analysis of hepatic α-Sma and Col1α1 in representative mice from each group (n = 4 per group). (F) Immunoblots and cumulative densitometric analysis of hepatic α-Sma and Col1α1 in representative mice from each group, CON + VEH (n = 4), CCl<sub>4</sub> + VEH (n = 5), and CCl<sub>4</sub> + TMX (n = 4). Gapdh was used as an internal control. All band densities were normalized versus Gapdh. (G) qRT-PCR analysis of α-Sma and Col1α1 in pHSCs isolated from livers of representative mice from each group (n = 3 per group). Results of relative expression values are graphed as mean ± s.e.m. (Student’s t-test; \* p < 0.05 vs. CON + VEH group, # p < 0.05 vs. CCl<sub>4</sub> + VEH group). (H) Immunoblots of Tgf-β and α-Sma in these cells. Gapdh was used as an internal control. Immunoblots shown represent one of three experiments with similar results.

Given that Tβ4 is associated with Hh signaling in HSC transdifferentiation [16], the activation of Hh signaling was examined in these mice. Although the mRNA levels of Ilk,

an activator of Smo, and pGsk-3 $\beta$ , an inactive form of Gsk-3 $\beta$  that degrades Gli2, were rarely changed among the groups, Ilk and pGsk-3 $\beta$  protein levels were significantly higher in the CCl<sub>4</sub> + VEH group than in the CON + VEH group, and this upregulation led to an increase in Smo and Gli2 at both the mRNA and protein levels in mice with fibrotic livers (Figure 3A,B). T $\beta$ 4 knockout, however, abrogated these significant increases. These expression changes in these mice were also verified in pHSCs and showed that pHSCs from the CCl<sub>4</sub> + TMX group had significantly lower levels of Ilk, pGsk-3 $\beta$ , Smo and Gli2 than those from the CON + VEH group (Figure 3C,D). Taken together, these findings display that HSC-specific T $\beta$ 4 deletion ameliorates CCl<sub>4</sub>-induced liver fibrosis and injury by suppressing Hh signaling in mice.

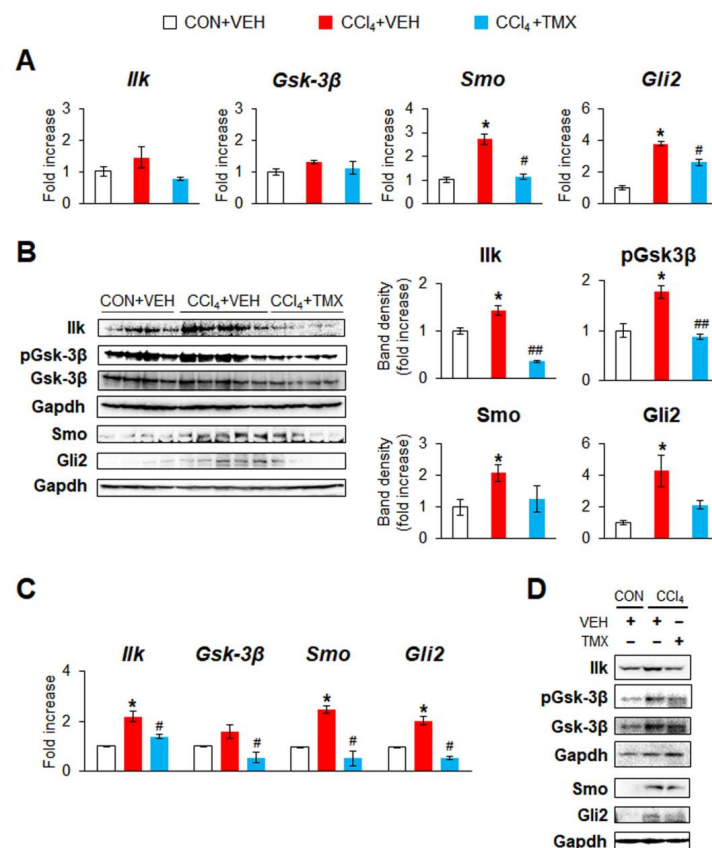


**Figure 3.** T $\beta$ 4 suppression in activated HSCs reduces expression of Hh signaling. (A) qRT-PCR analysis of Ilk, Gsk-3 $\beta$ , Smo, and Gli2 in the livers from representative DTG mice receiving corn oil (CON) + vehicle (VEH) ( $n = 3$ ), carbon tetrachloride (CCl<sub>4</sub>) + VEH ( $n = 3$ ), or CCl<sub>4</sub> + tamoxifen (TMX) ( $n = 4$ ). (B) Representative immunoblots and cumulative densitometric analysis of hepatic Ilk, phosphorylated (p) Gsk-3 $\beta$ , Gsk-3 $\beta$ , Smo, and Gli2 in representative mice from each group CON + VEH ( $n = 4$ ), CCl<sub>4</sub> + VEH ( $n = 5$ ), and CCl<sub>4</sub> + TMX ( $n = 4$ ). Gapdh was used as an internal control. All band densities were normalized versus Gapdh, except that pGsk-3 $\beta$  was normalized to total Gsk-3 $\beta$ . (C) qRT-PCR analysis of Ilk, Gsk-3 $\beta$ , Smo, and Gli2 in pHSCs isolated from livers of representative mice from each group ( $n = 3$  per group). Results of relative expression values are graphed as mean  $\pm$  s.e.m. (Student’s  $t$ -test; \*  $p < 0.05$  vs. CON + VEH group, #  $p < 0.05$ , ##  $p < 0.005$  vs. CCl<sub>4</sub> + VEH group). (D) Immunoblots of Ilk, pGsk-3 $\beta$ , Gsk-3 $\beta$ , Smo, and Gli2 in these cells. Gapdh was used as an internal control. Immunoblots shown represent one of three experiments with similar results.

### 3.3. Blocking T $\beta$ 4 in HSCs Attenuates Bile Duct Ligation (BDL)-Caused Liver Fibrosis in Mice

To further validate in vivo roles of T $\beta$ 4 in hepatic fibrosis, we employed bile duct ligation (BDL) as an additional animal model of liver fibrosis. CCl<sub>4</sub> is a chemical that damages hepatocytes and induces inflammation and fibrosis, whereas BDL is a surgical

method to induce the proliferation of biliary epithelial cells, followed by inflammation and fibrosis [22,26]. DTG mice underwent sham surgery or BDL for 3 weeks and were injected with VEH or TMX [22] (Figure 4A). As shown in the CCl<sub>4</sub> model, hepatic Tβ4 expression was greatly elevated in the BDL + VEH group compared with the Sham + VEH group, whereas this level was significantly alleviated in the BDL + TMX group compared with the BDL + VEH group, as measured by qRT-PCR and immunoblotting (Figure 4B,C). Immunostaining for Tβ4 presented that the accumulation of cells positive for Tβ4 in the liver sections from the BDL + TMX group was noticeably decreased in the BDL + TMX group (Figure 4D, top panel). Mice injured by BDL had severe liver damage, such as massive cell death, excessive inflammation, and increases in the LW/BW ratio and ALT/AST level compared with control mice subjected to sham operation (Figure 4D, middle panel, E, F). However, compared with mice in the BDL + VEH group, mice lacking Tβ4 exhibited significantly mild injury, although these mice were subjected to the BDL operation. In addition, hepatic fibrosis caused by BDL was remarkably ameliorated in the BDL + TMX group compared with the BDL + VEH group (Figure 4D bottom panel, G). TMX itself hardly impacted the liver in the sham surgery group (Figure S4). The amounts of α-Sma and Col1α1 were higher in the BDL + VEH group than the Sham + VEH group and were remarkably decreased in the BDL + TMX group (Figure 5A,B). The reduction in HSC activation in the BDL + TMX group was supported by immunostaining for α-Sma, which showed less accumulation of α-Sma-expressing HSCs in the BDL + TMX group than in the BDL + VEH group (Figure 5C). Compared with those in the Sham + VEH group, the protein levels of Ilk and pGsk-3β and the mRNA and protein levels of Smo and Gli2 were significantly enhanced in the BDL + VEH group with upregulated Tβ4, which was similar to the CCl<sub>4</sub> model. However, this expression noticeably declined in the BDL + TMX group with Tβ4 suppression (Figure 5D,E). These findings demonstrate that conditional disruption of Tβ4 in activated HSCs alleviates BDL-induced liver injury and fibrosis by inhibiting Hh signaling in mice.

### 3.4. Tβ4 Restoration Reverses the Effect of Tβ4 Depletion on Mitigating Liver Fibrosis

To verify the action of Tβ4 in activated HSCs and liver fibrosis in mice, exogenous Tβ4 was administered to CCl<sub>4</sub>-treated DTG mice to restore Tβ4 deficiency in these mice. To conditionally enhance Tβ4 re-expression in the livers of TMX-treated DTG mice, adeno-associated virus type-6 (AAV6), which has been reported to mainly target HSCs [24], was administered. After the 3rd injection of CCl<sub>4</sub>, DTG mice received a single intravenous administration of AAV6-Tβ4 or AAV6-control (AAV6-Con), and then residual TMX and CCl<sub>4</sub> injections were administered to these mice in an identical regimen (Figure 6A). The time point of AAV6 administration was determined based on previous studies [23,27,28].

AAV6-Tβ4 administration upregulated hepatic Tβ4 expression in the CCl<sub>4</sub> + TMX + AAV6-Tβ4 group, restoring it to a level similar to that in the CCl<sub>4</sub> + VEH + AAV6-Con group, as measured by qRT-PCR and immunoblot analysis (Figure 6B,C). The recovered Tβ4 level was supported by immunohistochemistry staining for Tβ4, which showed that Tβ4-expressing cells were noticeably increased in the livers in the CCl<sub>4</sub> + TMX + AAV6-Tβ4 group compared with the CCl<sub>4</sub> + TMX + AAV6-Con group (Figure 6D, top panel). To identify whether AAV6-mediated restoration of Tβ4 exacerbated liver damage in the context of fibrosis, we checked the liver morphology and degree of liver fibrosis in these mice. The improvements in liver morphology and function due to Tβ4 suppression were worsened by Tβ4 recovery in the CCl<sub>4</sub> + TMX + AAV6-Tβ4 group (Figure 6D, bottom panel, E,F). The amounts of α-Sma and Col1α1 were significantly elevated in the CCl<sub>4</sub> + TMX + AAV6-Tβ4 group compared with the CCl<sub>4</sub> + TMX + AAV6-Con group, and these levels in the CCl<sub>4</sub> + TMX + AAV6-Tβ4 group were similar to those in the CCl<sub>4</sub> + VEH + AAV6-Con group (Figure 7A,B). The accumulation of α-Sma-expressing cells and fibrotic nodules was more evident in the CCl<sub>4</sub> + TMX + AAV6-Tβ4 group than in the CCl<sub>4</sub> + TMX + AAV6-Con group (Figure 7C). Hepatic hydroxyproline levels confirmed that the CCl<sub>4</sub> + TMX + AAV6-Tβ4 group had markedly more liver fibrosis than the CCl<sub>4</sub> + TMX + AAV6-Con group

(Figure 7D). Consistent with the re-establishment of Tβ4 expression and liver fibrosis, activated Hh signaling was also observed. The levels of Ilk, pGsk-3β, Smo, and Gli2 were enhanced in the CCl<sub>4</sub> + TMX + AAV6-Tβ4 group compared with the CCl<sub>4</sub> + TMX + AAV6-Con group, as evaluated by qRT-PCR and immunoblotting (Figure 8A,B). These findings reveal that the restoration of Tβ4 in Tβ4-deficient HSCs activates Hh signaling and promotes liver fibrosis, indicating that Tβ4 is one of the main regulators of HSC activation and liver fibrosis.

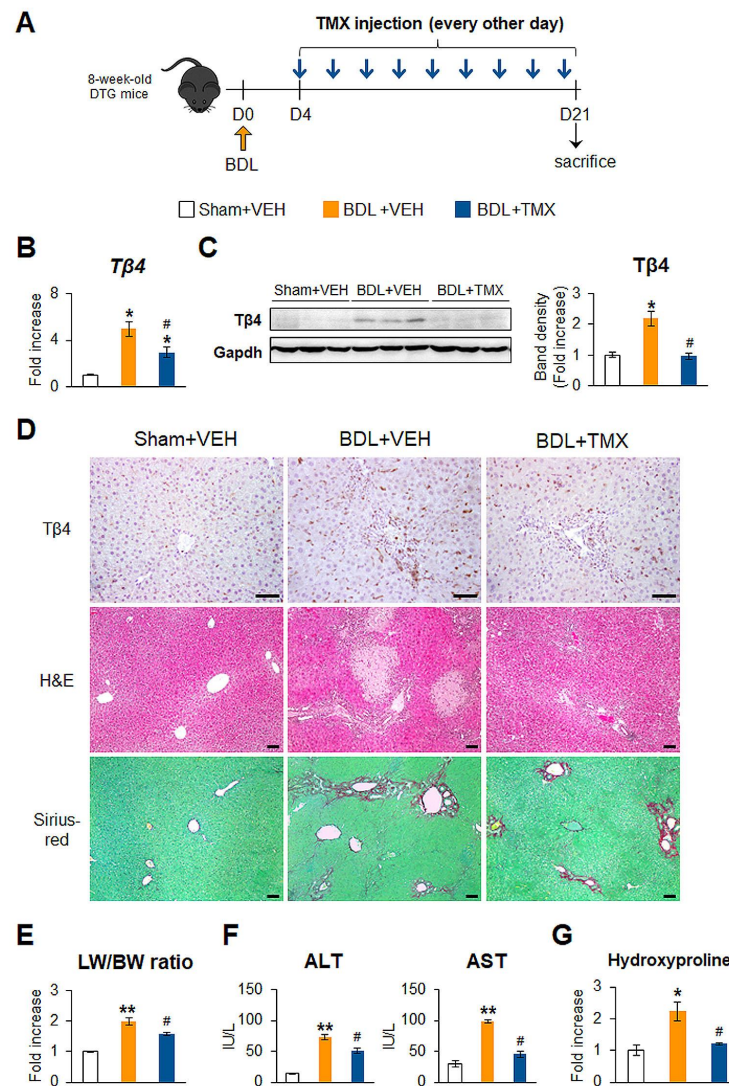


**Figure 4.** Tβ4 deficiency in HSCs attenuates BDL-induced liver injury and fibrosis. **(A)** Schematic diagram showing the timing of bile duct ligation (BDL) surgery and tamoxifen (TMX) injections into double-transgenic (DTG) mice. At 3 weeks after the surgery, all DTG mice receiving either vehicle (VEH) or TMX were sacrificed for harvesting tissue samples. **(B)** qRT-PCR of hepatic Tβ4 in representative DTG mice receiving sham surgery (Sham) + vehicle (VEH) (*n* = 3), BDL + VEH (*n* = 4), or BDL + TMX (*n* = 4). **(C)** Representative immunoblots and cumulative densitometric analysis of hepatic Tβ4 in representative mice from each group (*n* = 3 per group). Gapdh was used as an internal control. Band densities were normalized versus Gapdh. **(D)** Representative images of immunostaining for Tβ4, hematoxylin and eosin (H&E) staining, and Sirius red staining in liver sections of representative mice from each group (scale bar = 50 μm). **(E)** Relative ratio of liver weight to body weight (LW/BW), **(F)** serum levels of ALT and AST and **(G)** hepatic hydroxyproline contents in all mice. Results were graphed as mean ± s.e.m. (Student’s *t*-test; \* *p* < 0.05, \*\* *p* < 0.005 vs. Sham + VEH group, # *p* < 0.05 vs. BDL + VEH group).

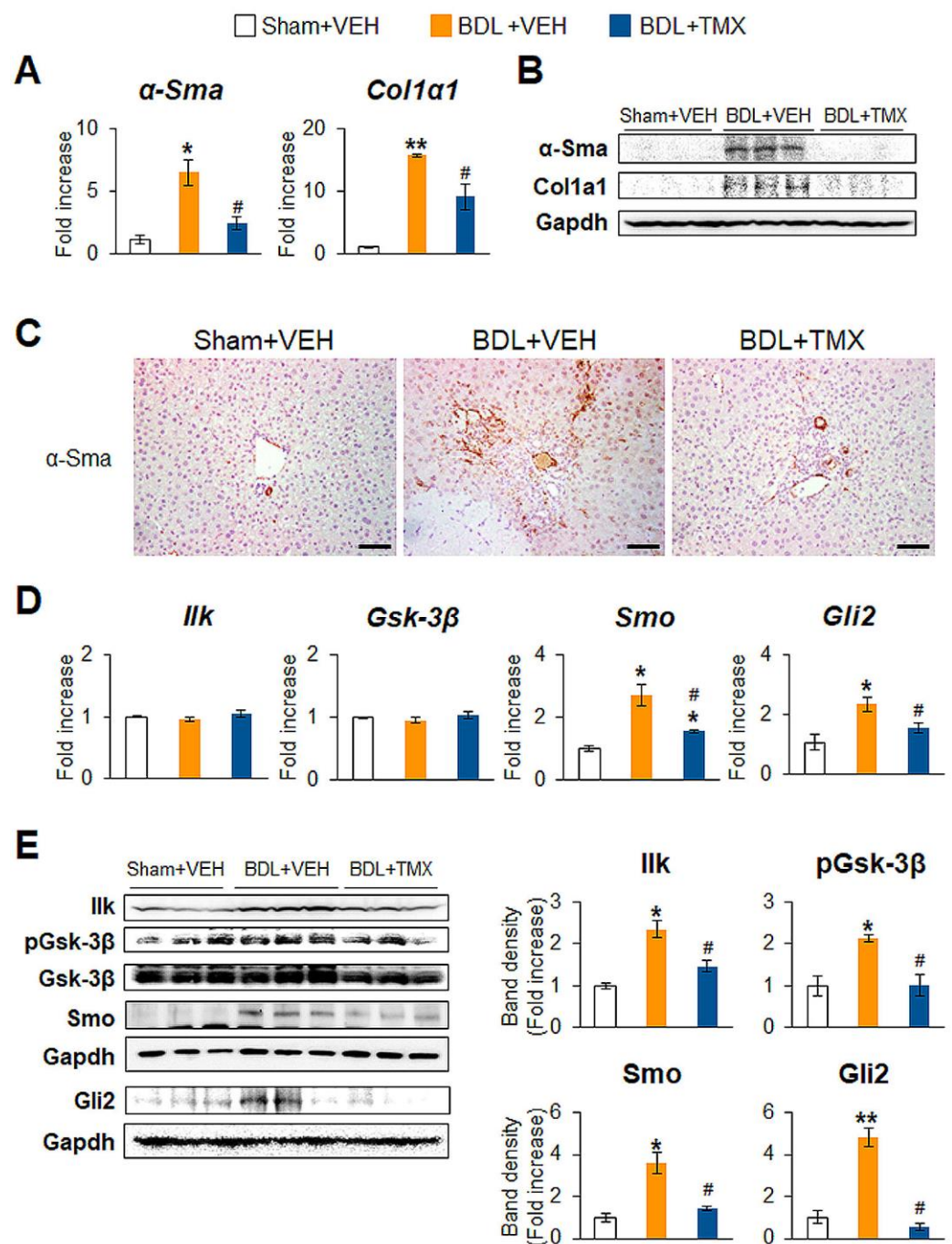


**Figure 5.** Deleting T $\beta$ 4 in HSCs downregulates fibrotic genes and Hh signaling in the liver damaged by BDL. (A) qRT-PCR analysis of  $\alpha$ -Sma and Col1 $\alpha$ 1 in liver tissues from representative DTG mice receiving Sham + VEH ( $n = 3$ ), BDL + VEH ( $n = 4$ ), or BDL + TMX ( $n = 4$ ). (B) Representative immunoblots of hepatic  $\alpha$ -Sma and Col1 $\alpha$ 1 in mice from representative mice from each group. Gapdh was used as an internal control. (C) Representative images of immunostaining for  $\alpha$ -Sma in liver sections of from representative mice from each group (scale bar = 50  $\mu$ m). (D) qRT-PCR analysis of hepatic Ilk, Gsk-3 $\beta$ , Smo, and Gli2 in the livers of representative mice from each group, Sham + VEH ( $n = 3$ ), BDL + VEH ( $n = 4$ ), and BDL + TMX ( $n = 4$ ). (E) Immunoblots and cumulative densitometric analysis of hepatic Ilk, phosphorylated (p) Gsk-3 $\beta$ , Gsk-3 $\beta$ , Smo, and Gli2 in representative mice from each group ( $n = 3$  per group). Gapdh was used as an internal control. All band densities were normalized versus Gapdh, except that pGsk-3 $\beta$  was normalized to total Gsk-3 $\beta$ . Results of relative expression values are graphed as mean  $\pm$  s.e.m. (Student's  $t$ -test; \*  $p < 0.05$ , \*\*  $p < 0.005$  vs. Sham + VEH group, #  $p < 0.05$  vs. BDL + VEH group).

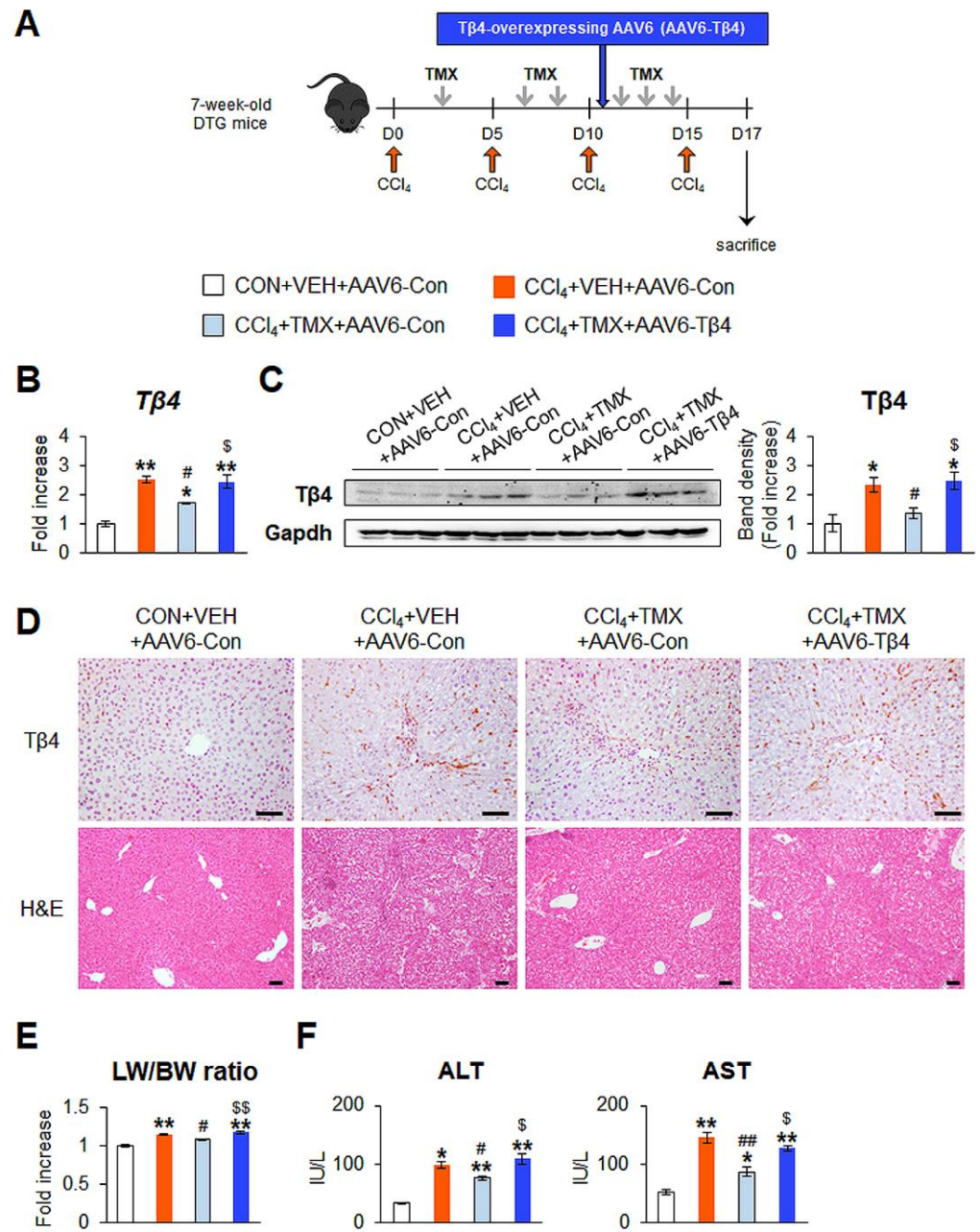


**Figure 6.** AAV6-mediated re-expression of Tβ4 worsens CCl<sub>4</sub>-induced liver damage in DTG mice treated with tamoxifen. (A) Schematic diagram showing the timing of CCl<sub>4</sub>, TMX, and Tβ4-expressing adeno-associated virus type-6 (AAV6) administrations into double-transgenic (DTG) mice. At 2 days after the last injection of CCl<sub>4</sub>, all DTG mice receiving corn oil (CON) + vehicle (VEH) + AAV6-Con, CCl<sub>4</sub> + VEH + AAV6-Con, CCl<sub>4</sub> + TMX + AAV6-Con, and CCl<sub>4</sub> + TMX + AAV6-Tβ4 were sacrificed. (B) qRT-PCR of Tβ4 in the livers from representative DTG mice receiving CON + VEH + AAV6-Con (n = 3), CCl<sub>4</sub> + VEH + AAV6-Con (n = 3), CCl<sub>4</sub> + TMX + AAV6-Con (n = 4), or CCl<sub>4</sub> + TMX + AAV6-Tβ4 (n = 4). (C) Representative immunoblots and cumulative densitometric analysis of hepatic Tβ4 in representative mice from each group (n = 3 per group). Gapdh was used as an internal control. Band densities were normalized versus Gapdh. (D) Representative images of immunostaining for Tβ4 and hematoxylin and eosin (H&E) staining in liver sections of representative mice from each group (scale bar = 50 μm). (E) Relative ratio of liver weight to body weight (LW/BW); (F) serum levels of ALT and AST in all mice from each group. Results were graphed as mean ± s.e.m. (Student's *t*-test; \* *p* < 0.05, \*\* *p* < 0.005 vs. CON + VEH + AAV6-Con group, # *p* < 0.05, ## *p* < 0.005 vs. CCl<sub>4</sub> + VEH + AAV6-Con group, \$ *p* < 0.05, \$\$ *p* < 0.005 vs. CCl<sub>4</sub> + TMX + AAV6-Con group).

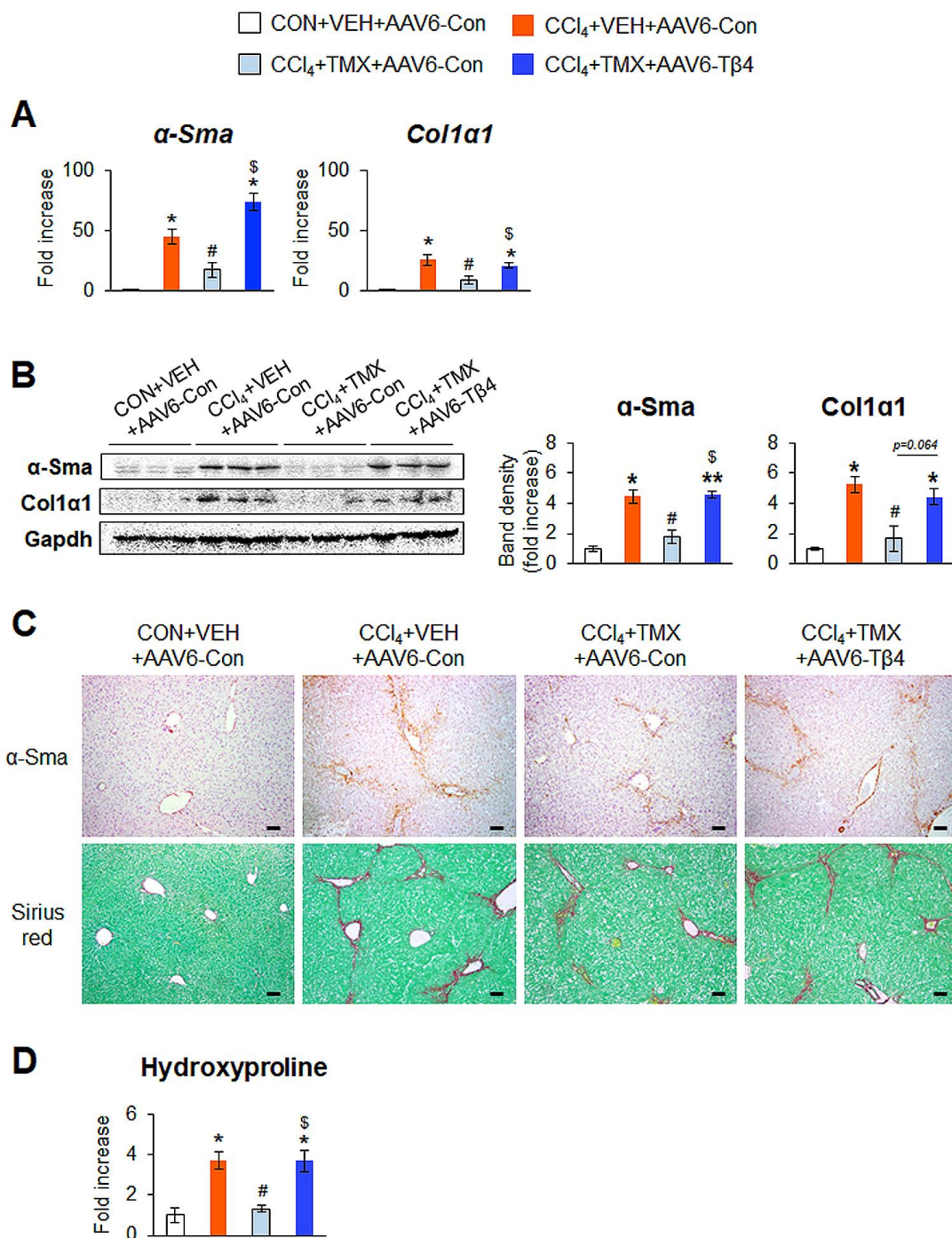


**Figure 7.** Re-expression of Tβ4 by AAV6-Tβ4 activates HSCs and aggravates liver fibrosis in tamoxifen-treated DTG mice. **(A)** qRT-PCR analysis of hepatic α-Sma and Col1α1 in representative DTG mice receiving CON + VEH + AAV6-Con (*n* = 3), CCl<sub>4</sub> + VEH + AAV6-Con (*n* = 3), CCl<sub>4</sub> + TMX + AAV6-Con (*n* = 4), or CCl<sub>4</sub> + TMX + AAV6-Tβ4 (*n* = 3). **(B)** Representative immunoblots and cumulative densitometric analysis of hepatic α-Sma and Col1α1 in representative mice from each group (*n* = 3 per group). Gapdh was used as an internal control. Band densities were normalized versus Gapdh. **(C)** Representative images of immunostaining for α-Sma and Sirius red staining in liver sections from each group (scale bar = 50 μm). **(D)** Hepatic hydroxyproline contents in livers of all mice from each group. Results were graphed as mean ± s.e.m. (Student’s *t*-test; \* *p* < 0.05, \*\* *p* < 0.005 vs. CON + VEH + AAV6-Con group, # *p* < 0.05 vs. CCl<sub>4</sub> + VEH + AAV6-Con group, \$ *p* < 0.05 vs. CCl<sub>4</sub> + TMX + AAV6-Con group).

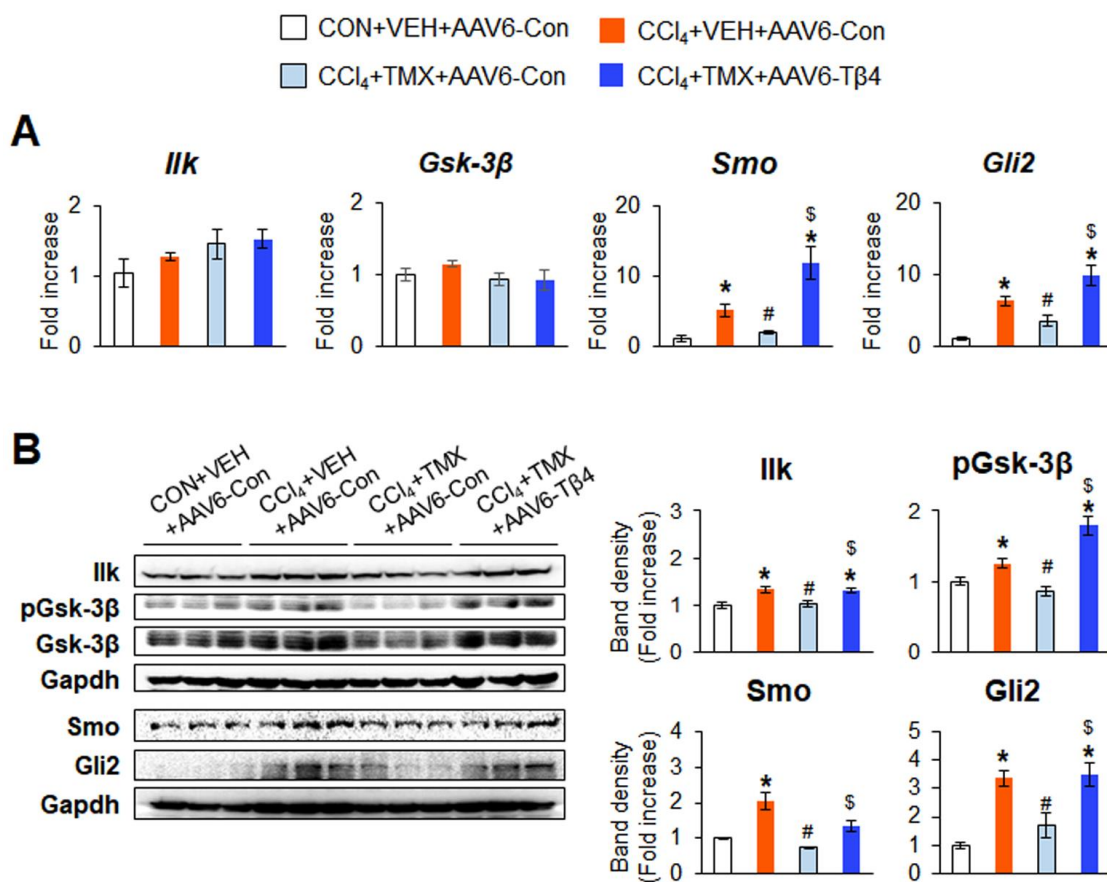


**Figure 8.** Re-expression of Tβ4 by AAV6 provokes activation of Hh signaling in tamoxifen-treated DTG mice. (A) qRT-PCR analysis of *Ilk*, *Gsk-3β*, *Smo*, and *Gli2* in the liver tissues from representative DTG mice receiving CON + VEH + AAV6-Con (*n* = 3), CCl<sub>4</sub> + VEH + AAV6-Con (*n* = 3), CCl<sub>4</sub> + TMX + AAV6-Con (*n* = 4), and CCl<sub>4</sub> + TMX + AAV6-Tβ4 (*n* = 3). Results of relative expression values are graphed as mean ± s.e.m. (B) Representative immunoblots and cumulative densitometric analysis of hepatic *Ilk*, phosphorylated (p) *Gsk-3β*, *Gsk-3β*, *Smo*, and *Gli2* in representative mice from each group (*n* = 3 per group). *Gapdh* was used as an internal control. All band densities were normalized versus *Gapdh*, except that p*Gsk-3β* was normalized to total *Gsk-3β*. Results of relative expression values are graphed as mean ± s.e.m. (Student’s *t*-test; \* *p* < 0.05 vs. CON + VEH + AAV6-Con group, # *p* < 0.05 vs. CCl<sub>4</sub> + VEH + AAV6-Con group, § *p* < 0.05 vs. CCl<sub>4</sub> + TMX + AAV6-Con).

#### 4. Discussion

Since HSCs are key modulators in the development of liver fibrosis, HSCs have been major targets for antifibrotic therapies [1,29]. Inhibiting HSC activation is considered the key strategy to reduce the number of ECM-producing cells and can prevent and treat liver fibrosis [2,29]. Thus, to unveil the functional effect of Tβ4 on HSC transdifferentiation in the liver, we used the two most widely used animal models of liver fibrosis: the CCl<sub>4</sub> model and the BDL model. α-Sma is the most well-known marker of activated/myofibroblastic HSCs, and these cells expressing α-Sma proliferate and accumulate in the CCl<sub>4</sub> or BDL model [22,23]. Based on our previous studies that showed that α-Sma-positive HSCs express Tβ4 in fibrotic livers [16,17], we used the TMX-inducible Cre/loxP system to conditionally knock out Tβ4 in α-Sma-expressing cells. In both the CCl<sub>4</sub> and BDL models, TMX injection significantly downregulated Tβ4 expression compared to that in the vehicle-injected group (Figures 1 and 4). Moreover, HSC-targeted Tβ4 deletion reduced the level of α-Sma and the deposition of fibrillar collagen, leading to a reduction in liver fibrosis (Figures 2, 4 and 5). These findings suggest that deleting Tβ4 in activated HSCs could be an effective strategy to suppress HSC activation and eventually reduce liver fibrosis.



Although two different experimental models of liver fibrosis were used to examine the *in vivo* function of T $\beta$ 4, the relatively short-term injection of CCl<sub>4</sub> (four CCl<sub>4</sub> injections for 20 days) compared with the classical CCl<sub>4</sub> injury model (CCl<sub>4</sub> injection for 6~10 weeks) is a limitation of the research. However, because long-term exposure to TMX itself is reported to be toxic to the liver and stomach [30–32], we had to adopt the short-term injection model of CCl<sub>4</sub> based on the TMX exposure period, which was verified in another study using the TMX-inducible Cre-loxP model system [23]. We confirmed severe hepatic damage including fibrosis in mice receiving a short-term injection of CCl<sub>4</sub>, and we confirmed that TMX itself hardly influenced our experimental system except for Cre activation (Figures S2–S4). The successful deletion of T $\beta$ 4 in HSCs and no harmful effects of T $\beta$ 4 on the uninjured liver support that the animal experimental design is appropriate. Nevertheless, further research is required to examine the long-term influences of T $\beta$ 4 on the progression of chronic liver fibrosis and cirrhosis to validate relevance of T $\beta$ 4 in a chronic model more closely reflecting human liver fibrosis.

T $\beta$ 4 was shown to regulate HSC activation through Hh signaling, an essential controller of HSC activation [16]. In particular, the Smo–Gli2 axis, an activator of Hh signaling, is crucial in orchestrating liver fibrosis [22,33–35]. During HSC activation, T $\beta$ 4 promoted the activation of the Smo–Gli2 axis by modulating the activity of ILK and pGSK-3 $\beta$  and directly interacting with Smo and Gli2 [16]. In line with these findings, an *in vivo* study using mice lacking T $\beta$ 4 in activated HSCs demonstrated that T $\beta$ 4 depletion in HSCs impaired the Hh activation. Although T $\beta$ 4 deletion downregulated only the protein but not the mRNA levels of ILK and pGSK-3 $\beta$  in whole liver tissues in the CCl<sub>4</sub> and BDL models (Figures 3 and 5), the data obtained from the pHSC experiments clearly showed that TMX-inducible T $\beta$ 4 deletion significantly reduced the mRNA levels of ILK and GSK-3 $\beta$  in these cells (Figure 3). In addition, given that T $\beta$ 4 is known to mainly regulate the stability of the ILK protein and the phosphorylation of GSK-3 $\beta$  [16,36–38], our data clearly suggest that T $\beta$ 4 regulates ILK and GSK-3 $\beta$ .

T $\beta$ 4 was initially recognized as a G-actin-binding protein and is capable of regulating cytoskeleton reorganization and cell motility [4,5,9]. Recently, novel functions of T $\beta$ 4 have been revealed based on its ability to impact various biological activities, such as cell survival, migration, repair, and angiogenesis [4,10,11,39]. However, most findings have been obtained from investigating the function of exogenous or synthetic T $\beta$ 4 that was applied extracellularly or in a paracrine manner [4,5,9]. A relatively small number of studies have paid attention to the *in vivo* functions of endogenous T $\beta$ 4. There have been several reports published studying the role of endogenous T $\beta$ 4 in heart and hair growth in T $\beta$ 4 transgenic mice, including ubiquitous knockout, tissue-specific knockout, or overexpression mice [40–43]. Our previous study showed that mice overexpressing T $\beta$ 4 were more susceptible to the development of liver fibrosis than WT mice [16]. The present study also demonstrates that HSC-specific deletion of T $\beta$ 4 prevents fibrosis in the liver, and this effect is reversed by the re-expression of T $\beta$ 4 in HSCs, confirming that endogenous T $\beta$ 4 expressed by activated HSCs has an *in vivo* function in facilitating HSC activation and liver fibrosis. The reason why our finding on the endogenous action of hepatic T $\beta$ 4 opposes the beneficial actions of exogenous T $\beta$ 4 shown by other studies remains unknown. However, it is highly possible that there is a difference between the effects of endogenous and exogenous T $\beta$ 4 [5]. Banerjee et al. reported that whole-body or cardiac-specific knockout of T $\beta$ 4 did not influence overall embryonic development, heart development, or adult cardiac function [42]. These data are also contrary to many other findings showing that exogenous T $\beta$ 4 administration improves cardiovascular function and repair [38,44–46]. Notably, in cancer studies, many reports have shown that T $\beta$ 4 is upregulated in breast, colorectal, and pancreatic cancer and is associated with poor prognosis [47–51]. Therefore, in advance of the therapeutic use of T $\beta$ 4, further studies and evidence are needed to determine the roles of endogenous T $\beta$ 4 and should discuss the potential use of exogenous or synthetic T $\beta$ 4 regarding the action of endogenous T $\beta$ 4.

In conclusion, our results show that HSC-targeted T $\beta$ 4 deletion reduces liver fibrosis *in vivo* by suppressing Hh signaling and that T $\beta$ 4 regulates HSC activation during liver fibrosis, suggesting that T $\beta$ 4 could be a good target for controlling HSC activation in the development of effective therapeutics for chronic liver disease. In addition, the T $\beta$ 4-flox mice that we generated might be a useful tool for investigating the unrevealed functions of endogenous T $\beta$ 4 in a tissue- and/or cell-specific manner and contribute to the safe therapeutic application of T $\beta$ 4 to the clinic.

**Supplementary Materials:** The following supporting information can be downloaded at: <https://www.mdpi.com/article/10.3390/cells12121658/s1>, Figure S1: Design of guide RNAs for CRISPR/Cas9 genome editing; Figure S2: Mice receiving four injections of CCl<sub>4</sub> have liver damage with fibrosis and increased level of T $\beta$ 4 and Hh signaling; Figure S3: Tamoxifen rarely impacts the liver treated with corn-oil; Figure S4: Tamoxifen hardly influences the liver subjected to sham surgery; Table S1: Primer sequences used for real-time PCR.

**Author Contributions:** J.K.: data curation, formal analysis, funding acquisition, investigation, methodology, software, validation, visualization, writing—original draft. C.L.: data curation, formal analysis, software, investigation, methodology, funding acquisition, visualization. J.H.: data curation, formal analysis, investigation, methodology, visualization. H.J.: data curation, formal analysis, investigation, methodology, visualization. S.W.: data curation, formal analysis, investigation, methodology. Y.H.C.: investigation, validation. Y.J.: conceptualization, funding acquisition, project administration, resources, supervision, writing—original draft. All authors have read and agreed to the published version of the manuscript.

**Funding:** This work was supported by Y.J. and the National Research Foundation (NRF) of Korea funded by the Korean government (MEST) to J.K. (No. 2019R1I1A1A01057379) and NRF of Korea funded by the Korean government (MEST) to C.L. (No. 2022R1C1C2008830).

**Institutional Review Board Statement:** Animal care and surgical procedures were approved by the Pusan National University–Institutional Animal Care and Use Committee and carried out in accordance with the provisions of the National Institutes of Health Guide for the Care and Use of Laboratory Animals (Approval Number PNU-2016-1286; 10-26-16, and PNU-2020-2652; 06-30-20).

**Informed Consent Statement:** Not applicable.

**Data Availability Statement:** All data were included in this paper.

**Conflicts of Interest:** The authors declare no conflict of interest.

## References

1. Bataller, R.; Brenner, D.A. Liver fibrosis. *J. Clin. Investig.* **2005**, *115*, 209–218. [[CrossRef](#)] [[PubMed](#)]
2. Reeves, H.L.; Friedman, S.L. Activation of hepatic stellate cells—A key issue in liver fibrosis. *Front. Biosci.* **2002**, *7*, d808–d826. [[CrossRef](#)]
3. Yin, C.; Evason, K.J.; Asahina, K.; Stainier, D.Y. Hepatic stellate cells in liver development, regeneration, and cancer. *J. Clin. Investig.* **2013**, *123*, 1902–1910. [[CrossRef](#)]
4. Goldstein, A.L.; Hannappel, E.; Kleinman, H.K. Thymosin beta4: Actin-sequestering protein moonlights to repair injured tissues. *Trends Mol. Med.* **2005**, *11*, 421–429. [[CrossRef](#)] [[PubMed](#)]
5. Kim, J.; Jung, Y. Potential role of thymosin Beta 4 in liver fibrosis. *Int. J. Mol. Sci.* **2015**, *16*, 10624–10635. [[CrossRef](#)] [[PubMed](#)]
6. Vartiainen, N.; Pyykönen, I.; Hökfelt, T.; Koistinaho, J. Induction of thymosin beta(4) mRNA following focal brain ischemia. *Neuroreport* **1996**, *7*, 1613–1616. [[CrossRef](#)] [[PubMed](#)]
7. Zuo, Y.; Chun, B.; Potthoff, S.A.; Kazi, N.; Brolin, T.J.; Orhan, D.; Yang, H.C.; Ma, L.J.; Kon, V.; Myöhänen, T.; et al. Thymosin  $\beta$ 4 and its degradation product, Ac-SDKP, are novel reparative factors in renal fibrosis. *Kidney Int.* **2013**, *84*, 1166–1175. [[CrossRef](#)]
8. De Santis, M.; Inzitari, R.; Bosello, S.L.; Peluso, G.; Fanali, C.; Iavarone, F.; Zizzo, G.; Bocci, M.; Cabras, T.; Messana, I.; et al.  $\beta$ -Thymosins and interstitial lung disease: Study of a scleroderma cohort with a one-year follow-up. *Respir. Res.* **2011**, *12*, 22. [[CrossRef](#)]
9. Xing, Y.; Ye, Y.; Zuo, H.; Li, Y. Progress on the Function and Application of Thymosin  $\beta$ 4. *Front. Endocrinol.* **2021**, *12*, 767785. [[CrossRef](#)]
10. Malinda, K.M.; Sidhu, G.S.; Mani, H.; Banaudha, K.; Maheshwari, R.K.; Goldstein, A.L.; Kleinman, H.K. Thymosin  $\beta$ 4 accelerates wound healing. *J. Investig. Dermatol.* **1999**, *113*, 364–368. [[CrossRef](#)]

11. Treadwell, T.; Kleinman, H.K.; Crockford, D.; Hardy, M.A.; Guarnera, G.T.; Goldstein, A.L. The regenerative peptide thymosin  $\beta$ 4 accelerates the rate of dermal healing in preclinical animal models and in patients. *Ann. N. Y. Acad. Sci.* **2012**, *1270*, 37–44. [[CrossRef](#)]
12. Philp, D.; Badamchian, M.; Scheremeta, B.; Nguyen, M.; Goldstein, A.L.; Kleinman, H.K. Thymosin beta 4 and a synthetic peptide containing its actin-binding domain promote dermal wound repair in db/db diabetic mice and in aged mice. *Wound Repair. Regen.* **2003**, *11*, 19–24. [[CrossRef](#)]
13. Sosne, G.; Ousler, G.W. Thymosin beta 4 ophthalmic solution for dry eye: A randomized, placebo-controlled, Phase II clinical trial conducted using the controlled adverse environment (CAE™) model. *Clin. Ophthalmol.* **2015**, *9*, 877–884. [[CrossRef](#)] [[PubMed](#)]
14. Sosne, G.; Dunn, S.P.; Kim, C. Thymosin  $\beta$ 4 significantly improves signs and symptoms of severe dry eye in a phase 2 randomized trial. *Cornea* **2015**, *34*, 491–496. [[CrossRef](#)] [[PubMed](#)]
15. Dunn, S.P.; Heidemann, D.G.; Chow, C.Y.; Crockford, D.; Turjman, N.; Angel, J.; Allan, C.B.; Sosne, G. Treatment of chronic nonhealing neurotrophic corneal epithelial defects with thymosin beta 4. *Arch. Ophthalmol.* **2010**, *128*, 636–638. [[CrossRef](#)] [[PubMed](#)]
16. Kim, J.; Hyun, J.; Wang, S.; Lee, C.; Lee, J.W.; Moon, E.Y.; Cha, H.; Diehl, A.M.; Jung, Y. Thymosin beta-4 regulates activation of hepatic stellate cells via hedgehog signaling. *Sci. Rep.* **2017**, *7*, 3815. [[CrossRef](#)]
17. Kim, J.; Wang, S.; Hyun, J.; Choi, S.S.; Cha, H.; Ock, M.; Jung, Y. Hepatic stellate cells express thymosin Beta 4 in chronically damaged liver. *PLoS ONE* **2015**, *10*, e0122758. [[CrossRef](#)] [[PubMed](#)]
18. Barnaeva, E.; Nadezhda, A.; Hannappel, E.; Sjogren, M.H.; Rojkind, M. Thymosin beta4 upregulates the expression of hepatocyte growth factor and downregulates the expression of PDGF-beta receptor in human hepatic stellate cells. *Ann. N. Y. Acad. Sci.* **2007**, *1112*, 154–160. [[CrossRef](#)]
19. Reyes-Gordillo, K.; Shah, R.; Arellanes-Robledo, J.; Rojkind, M.; Lakshman, M.R. Protective effects of thymosin  $\beta$ 4 on carbon tetrachloride-induced acute hepatotoxicity in rats. *Ann. N. Y. Acad. Sci.* **2012**, *1269*, 61–68. [[CrossRef](#)] [[PubMed](#)]
20. Reyes-Gordillo, K.; Shah, R.; Popratiloff, A.; Fu, S.; Hindle, A.; Brody, F.; Rojkind, M. Thymosin- $\beta$ 4 (T $\beta$ 4) blunts PDGF-dependent phosphorylation and binding of AKT to actin in hepatic stellate cells. *Am. J. Pathol.* **2011**, *178*, 2100–2108. [[CrossRef](#)]
21. Wendling, O.; Bornert, J.M.; Chambon, P.; Metzger, D. Efficient temporally-controlled targeted mutagenesis in smooth muscle cells of the adult mouse. *Genesis* **2009**, *47*, 14–18. [[CrossRef](#)] [[PubMed](#)]
22. Michelotti, G.A.; Xie, G.; Swiderska, M.; Choi, S.S.; Karaca, G.; Krüger, L.; Premont, R.; Yang, L.; Syn, W.K.; Metzger, D.; et al. Smoothed is a master regulator of adult liver repair. *J. Clin. Investig.* **2013**, *123*, 2380–2394. [[CrossRef](#)]
23. Troeger, J.S.; Mederacke, I.; Gwak, G.Y.; Dapito, D.H.; Mu, X.; Hsu, C.C.; Pradere, J.P.; Friedman, R.A.; Schwabe, R.F. Deactivation of hepatic stellate cells during liver fibrosis resolution in mice. *Gastroenterology* **2012**, *143*, 1073–1083.e22. [[CrossRef](#)]
24. Rezvani, M.; Español-Suñer, R.; Malato, Y.; Dumont, L.; Grimm, A.A.; Kienle, E.; Bindman, J.G.; Wiedtke, E.; Hsu, B.Y.; Naqvi, S.J.; et al. In Vivo Hepatic Reprogramming of Myofibroblasts with AAV Vectors as a Therapeutic Strategy for Liver Fibrosis. *Cell. Stem Cell.* **2016**, *18*, 809–816. [[CrossRef](#)] [[PubMed](#)]
25. Hyun, J.; Wang, S.; Kim, J.; Rao, K.M.; Park, S.Y.; Chung, I.; Ha, C.S.; Kim, S.W.; Yun, Y.H.; Jung, Y. MicroRNA-378 limits activation of hepatic stellate cells and liver fibrosis by suppressing Gli3 expression. *Nat. Commun.* **2016**, *7*, 10993. [[CrossRef](#)] [[PubMed](#)]
26. Yanguas, S.C.; Cogliati, B.; Willebrords, J.; Maes, M.; Colle, I.; van den Bossche, B.; de Oliveira, C.; Andraus, W.; Alves, V.A.F.; Leclercq, I.; et al. Experimental models of liver fibrosis. *Arch. Toxicol.* **2016**, *90*, 1025–1048. [[CrossRef](#)]
27. Zincarelli, C.; Soltys, S.; Rengo, G.; Rabinowitz, J.E. Analysis of AAV serotypes 1–9 mediated gene expression and tropism in mice after systemic injection. *Mol. Ther.* **2008**, *16*, 1073–1080. [[CrossRef](#)] [[PubMed](#)]
28. Bottani, E.; Giordano, C.; Civiletto, G.; Di Meo, I.; Auricchio, A.; Ciusani, E.; Marchet, S.; Lamperti, C.; d’Amati, G.; Viscomi, C.; et al. AAV-mediated liver-specific MPV17 expression restores mtDNA levels and prevents diet-induced liver failure. *Mol. Ther.* **2014**, *22*, 10–17. [[CrossRef](#)] [[PubMed](#)]
29. Higashi, T.; Friedman, S.L.; Hoshida, Y. Hepatic stellate cells as key target in liver fibrosis. *Adv. Drug. Deliv. Rev.* **2017**, *121*, 27–42. [[CrossRef](#)] [[PubMed](#)]
30. Huh, W.J.; Khurana, S.S.; Geahlen, J.H.; Kohli, K.; Waller, R.A.; Mills, J.C. Tamoxifen induces rapid, reversible atrophy, and metaplasia in mouse stomach. *Gastroenterology* **2012**, *142*, 21–24.e27. [[CrossRef](#)]
31. Gao, F.F.; Lv, J.W.; Wang, Y.; Fan, R.; Li, Q.; Zhang, Z.; Wei, L. Tamoxifen induces hepatotoxicity and changes to hepatocyte morphology at the early stage of endocrinotherapy in mice. *Biomed. Rep.* **2016**, *4*, 102–106. [[CrossRef](#)]
32. Burclaff, J.; Osaki, L.H.; Liu, D.; Goldenring, J.R.; Mills, J.C. Targeted Apoptosis of Parietal Cells Is Insufficient to Induce Metaplasia in Stomach. *Gastroenterology* **2017**, *152*, 762–766.e7. [[CrossRef](#)]
33. Yu, F.; Zheng, Y.; Hong, W.; Chen, B.; Dong, P.; Zheng, J. MicroRNA-200a suppresses epithelial-to-mesenchymal transition in rat hepatic stellate cells via GLI family zinc finger 2. *Mol. Med. Rep.* **2015**, *12*, 8121–8128. [[CrossRef](#)]
34. Sicklick, J.K.; Li, Y.X.; Choi, S.S.; Qi, Y.; Chen, W.; Bustamante, M.; Huang, J.; Zdanowicz, M.; Camp, T.; Torbenson, M.S.; et al. Role for hedgehog signaling in hepatic stellate cell activation and viability. *Lab. Investig.* **2005**, *85*, 1368–1380. [[CrossRef](#)] [[PubMed](#)]
35. Chen, Y.; Choi, S.S.; Michelotti, G.A.; Chan, I.S.; Swiderska-Syn, M.; Karaca, G.F.; Xie, G.; Moylan, C.A.; Garibaldi, F.; Premont, R.; et al. Hedgehog controls hepatic stellate cell fate by regulating metabolism. *Gastroenterology* **2012**, *143*, 1319–1329.e1311. [[CrossRef](#)] [[PubMed](#)]
36. Huang, H.C.; Hu, C.H.; Tang, M.C.; Wang, W.S.; Chen, P.M.; Su, Y. Thymosin beta4 triggers an epithelial-mesenchymal transition in colorectal carcinoma by upregulating integrin-linked kinase. *Oncogene* **2007**, *26*, 2781–2790. [[CrossRef](#)]

37. Ryu, Y.K.; Lee, Y.S.; Lee, G.H.; Song, K.S.; Kim, Y.S.; Moon, E.Y. Regulation of glycogen synthase kinase-3 by thymosin beta-4 is associated with gastric cancer cell migration. *Int. J. Cancer* **2012**, *131*, 2067–2077. [[CrossRef](#)]
38. Bock-Marquette, I.; Saxena, A.; White, M.D.; Dimaio, J.M.; Srivastava, D. Thymosin beta4 activates integrin-linked kinase and promotes cardiac cell migration, survival and cardiac repair. *Nature* **2004**, *432*, 466–472. [[CrossRef](#)]
39. Cha, H.J.; Jeong, M.J.; Kleinman, H.K. Role of thymosin beta4 in tumor metastasis and angiogenesis. *J. Natl. Cancer Inst.* **2003**, *95*, 1674–1680. [[CrossRef](#)] [[PubMed](#)]
40. Gao, X.Y.; Hou, F.; Zhang, Z.P.; Nuo, M.T.; Liang, H.; Cang, M.; Wang, Z.G.; Wang, X.; Xu, T.; Yan, L.Y.; et al. Role of thymosin beta 4 in hair growth. *Mol. Genet. Genomics* **2016**, *291*, 1639–1646. [[CrossRef](#)]
41. Gao, X.; Liang, H.; Hou, F.; Zhang, Z.; Nuo, M.; Guo, X.; Liu, D. Thymosin Beta-4 Induces Mouse Hair Growth. *PLoS ONE* **2015**, *10*, e0130040. [[CrossRef](#)] [[PubMed](#)]
42. Banerjee, I.; Zhang, J.; Moore-Morris, T.; Lange, S.; Shen, T.; Dalton, N.D.; Gu, Y.; Peterson, K.L.; Evans, S.M.; Chen, J. Thymosin beta 4 is dispensable for murine cardiac development and function. *Circ. Res.* **2012**, *110*, 456–464. [[CrossRef](#)] [[PubMed](#)]
43. Munshaw, S.; Bruche, S.; Redpath, A.N.; Jones, A.; Patel, J.; Dubé, K.N.; Lee, R.; Hester, S.S.; Davies, R.; Neal, G.; et al. Thymosin  $\beta$ 4 protects against aortic aneurysm via endocytic regulation of growth factor signaling. *J. Clin. Investig.* **2021**, *131*, e127884. [[CrossRef](#)] [[PubMed](#)]
44. Smart, N.; Risebro, C.A.; Melville, A.A.; Moses, K.; Schwartz, R.J.; Chien, K.R.; Riley, P.R. Thymosin beta4 induces adult epicardial progenitor mobilization and neovascularization. *Nature* **2007**, *445*, 177–182. [[CrossRef](#)]
45. Hinkel, R.; El-Aouni, C.; Olson, T.; Horstkotte, J.; Mayer, S.; Müller, S.; Willhauck, M.; Spitzweg, C.; Gildehaus, F.J.; Münzing, W.; et al. Thymosin beta4 is an essential paracrine factor of embryonic endothelial progenitor cell-mediated cardioprotection. *Circulation* **2008**, *117*, 2232–2240. [[CrossRef](#)] [[PubMed](#)]
46. Bock-Marquette, I.; Srivastava, S.; Pipes, G.C.; Thatcher, J.E.; Blystone, A.; Shelton, J.M.; Galindo, C.L.; Melegh, B.; Srivastava, D.; Olson, E.N.; et al. Thymosin beta4 mediated PKC activation is essential to initiate the embryonic coronary developmental program and epicardial progenitor cell activation in adult mice in vivo. *J. Mol. Cell. Cardiol.* **2009**, *46*, 728–738. [[CrossRef](#)]
47. Yoon, S.Y.; Lee, H.R.; Park, Y.; Kim, J.H.; Kim, S.Y.; Yoon, S.R.; Lee, W.J.; Cho, B.J.; Min, H.; Bang, J.W.; et al. Thymosin  $\beta$ 4 expression correlates with lymph node metastasis through hypoxia inducible factor- $\alpha$  induction in breast cancer. *Oncol. Rep.* **2011**, *25*, 23–31.
48. Zhang, Y.; Feurino, L.W.; Zhai, Q.; Wang, H.; Fisher, W.E.; Chen, C.; Yao, Q.; Li, M. Thymosin Beta 4 is overexpressed in human pancreatic cancer cells and stimulates proinflammatory cytokine secretion and JNK activation. *Cancer Biol. Ther.* **2008**, *7*, 419–423. [[CrossRef](#)] [[PubMed](#)]
49. Chi, L.H.; Chang, W.M.; Chang, Y.C.; Chan, Y.C.; Tai, C.C.; Leung, K.W.; Chen, C.L.; Wu, A.T.; Lai, T.C.; Li, Y.J.; et al. Global Proteomics-based Identification and Validation of Thymosin Beta-4 X-Linked as a Prognostic Marker for Head and Neck Squamous Cell Carcinoma. *Sci. Rep.* **2017**, *7*, 9031. [[CrossRef](#)]
50. Kang, Y.J.; Jo, J.O.; Ock, M.S.; Chang, H.K.; Lee, S.H.; Ahn, B.K.; Baek, K.W.; Choi, Y.H.; Kim, W.J.; Leem, S.H.; et al. Thymosin  $\beta$ 4 was upregulated in recurrent colorectal cancers. *J. Clin. Pathol.* **2014**, *67*, 188–190. [[CrossRef](#)]
51. Nemolato, S.; Restivo, A.; Cabras, T.; Coni, P.; Zorcolo, L.; Orrù, G.; Fanari, M.; Cau, F.; Gerosa, C.; Fanni, D.; et al. Thymosin  $\beta$  4 in colorectal cancer is localized predominantly at the invasion front in tumor cells undergoing epithelial mesenchymal transition. *Cancer Biol. Ther.* **2012**, *13*, 191–197. [[CrossRef](#)] [[PubMed](#)]

**Disclaimer/Publisher’s Note:** The statements, opinions and data contained in all publications are solely those of the individual author(s) and contributor(s) and not of MDPI and/or the editor(s). MDPI and/or the editor(s) disclaim responsibility for any injury to people or property resulting from any ideas, methods, instructions or products referred to in the content.